Electrochemical and spectroscopic investigations of redox interactions between aqueous selenium species and galena surfaces in acidic conditions

Peter Cook

ABSTRACT

As a redox sensitive element, the speciation and, therefore, the behavior of selenium in the geochemical environment can be affected by interactions with semiconducting minerals that can mediate redox reactions on the mineral surface. To determine the capacity of the sulfide mineral galena (PbS) to mediate such reactions, voltammetry was performed with powdered galena as working electrode in powder microelectrode (PME) experiments. Current/voltage (I/V) curves are generated using this setup where the voltage of a current peak can be related to the potential (Eh) of a specific redox transition and the current is indicative of the intensity and thus the kinetics of the reaction. At pH 4.6, three anodic (oxidizing) and cathodic (reducing) peaks in current were identified comprising three different redox couples assigned to

(1) $HSeO_3^- + 7H^+ + 6e^- \rightarrow H_2Se + 3H_2O$ at 0.0 V,

(2) $HSeO_3^- + H_2Se + 2e^- + 2H^+ \rightarrow 2Se^0 + 3H_2O$ at −430 mV, and

(3) $Se^0 + 2e^- + 2H^+ \rightarrow H_2Se$ at −560 mV.

Reversibility of all three couples was affected by the loss of cathodically produced H_2Se to the solution phase. The oxidation of Se^{4+} to some higher oxidation state, presumably Se^{6+}, was identified at 400 mV; however, assignment of the anodic feature could not be made due to the lack of a corresponding cathodic feature likely due to the electrochemical inactivity of Se^{6+}. XPS analysis revealed the formation of Se^0, likely of the black variety, after polarization at −125 mV attributed to the conproportionation of Se^{4+} and Se^{2-} species in solution. In contrast, red Se^0 was formed after polarization at −490 mV which was attributed to conproportionation mediated by the PbS surface. The latter process produces a voltammetric signal whereas the former process is not be detectable by voltammetry. Pb 4f and S 2p XPS spectra exhibited no correlation with the Se 3d spectra suggesting the lack of participation of PbS constituents in the redox transitions of selenium. In other words, PbS merely acts as a semiconductor mediating electron transfer and not as a source of electron for the reduction of selenite.

This study also proposes a novel technique for assessing reaction kinetics strictly using voltammetric data for estimating reaction rates, rate laws, and the number of participating PbS

surface sites occupied by selenium atoms during forward reactions. For example, for the reduction of bi-selenite to selenide at pH 4.6, the reaction equation can be written as:

$HSeO_3^- + 7H^+ + 6e^- \rightarrow H_2Se + 3H_2O \quad E^o = 387$ mV

The rate equation can be written as:

$r = k\,[HSeO_3^-]\,[e^-]^6\,[H^+]^7$ with a rate constant of about $8.8 \cdot 10^{20}$ $s^{-1}mol^{-13}$.

While redox reaction can produce or consume hydronium in solution, this process can change the pH and produce pH gradients in a certain volume around the PME. This study proposes a mechanism to quantify this pH change (from 4.6 to 4.8 for the reaction shown above) within a reaction volume which is on the order of 1-2 mm around the PME which is 0.1 mm in diameter. This information is important to evaluate diffusion kinetics about the reactive area during the redox process, which may control the overall reaction kinetics and to semi-quantify pH gradients that occur and are close-to impossible to measure in the pores of soils under environmental conditions.

1 INTRODUCTION

While a vital nutrient in low concentrations, the capacity of selenium to act as a toxic contaminant has been evinced by cases such as the Kesterson reservoir in California where high concentrations of selenium in sediments and aquatic systems have led to increased wildlife mortality rates and birth defects (Dubrovksy *et al.*, 1990; Wu, 2003). Owing to its chemical similarity to sulfur, such hazardous accumulations in the environment are often linked to the weathering of coal (Naftz and Rice, 1989) and selenium-bearing sulfide minerals (Clark and Johnson, 2011; Yudovich *et al.*, 2005). As a product of the nuclear fuel-cycle, selenium may also be introduced to the environment through effluents as the long-lived radionuclide ^{79}Se (Martinez-Torrents *et al.*, 2015).

Regardless of its source, the mobility of selenium in the geochemical environment is controlled by its oxidation state, which dictates factors such as sorption affinities and solubility (Fig. 1). For instance, Se^{6+} and Se^{4+} species are dominant under oxidizing conditions and are not only more bioavailable and toxic than reduced forms, but also more soluble granting them greater mobility (Clark and Johnson, 2011). Compared to Se^{4+}, Se^{6+} exhibits limited sorption (Duc *et al.*, 2003; Martinez *et al.*, 2006) and is commonly described as electrochemically inactive (Espinosa *et al.*, 1992; Han *et al.*, 2011; Han *et al.*, 2012; Jordan *et al.*, 2011; Kazacos

and Miller, 1980; Lange and van den Berg, 2000; Pourbaix, 1974; Saji and Lee, 2013). As a result, the mobility of Se^{4+} is more susceptible to limitations than Se^{6+} (Dhillon and Dhillon, 2000; Dubrovsky *et al.*, 1990; Naftz and Rice, 1989) and dominance of Se^{6+} over Se^{4+} in aquatic systems is often reported (Clark and Johnson, 2011; Dubrovsky *et al.*, 1990; Naftz and Rice, 1989). Under reducing conditions, selenium is found as various Se^{2-} species in addition to insoluble Se^0. While Se^{2-} can occur in the soluble H_2Se system, it also occurs as insoluble metallic selenides such as clausthalite (PbSe) or ferroselite ($FeSe_2$).

Semiconducting minerals such as PbS are not only ubiquitous in the natural environment, but also common electron sources and sinks. Consequently, interactions between selenium and PbS pose the chance for mobilization or immobilization by mediating redox reactions, which alter the speciation of selenium and therefore its behavior. In the literature, however, electrochemical investigations of selenium have mainly been limited to interactions with materials such as gold (Bougouma *et al.*, 2013; Cabral *et al.*, 2010; Ivandini and Einaga, 2013; Kowalik, 2014; Maranowski *et al.*, 2015; Solaliendres *et al.*, 2008; Wei *et al.*, 1994), platinum (Santos and Machado, 2004; Feliu *et al.*, 1993), and silver (Kazacos and Miller, 1980; Kowalik, 2014) offering little geochemical relevance. Studies that do involve interactions with mineral surfaces have typically been limited to batch chemistry studies (*i.e.*, non-electrochemical) with minerals such as pyrite (Curti *et al.*, 2012; Han *et al.*, 2012; Naveau *et al.*, 2007), apatite (Duc *et al.*, 2003), and magnetite (Martinez *et al.*, 2006).

The goal of the current study is to investigate the capacity of PbS to mediate selenium redox reactions, which to our knowledge, is lacking in the literature. For this purpose, this study will combine electrochemical methods to identify selenium-related redox reactions characterized with respect to factors such as reversibility, influence of pH, and kinetics. Spectroscopic methods are then used to confirm such reactions. Results from this study will help determine the ability for PbS to alter the behavior of selenium in the geochemical environment.

2 METHODS

2.1 Sample characterization

PbS sourced from Missouri was characterized using EDS primed to 15 kV and 112.6 µA (Fig. 2). In addition to Pb and S, Cu impurities were detected which is commonly found in PbS originating from Missouri (Kim *et al.*, 1994; Laajalehto *et al.*, 1997; Wittstock *et al.*, 1996).

2.2 Voltammetry

Voltammetry was conducted in a conventional 3-electrode cell controlled by an EG&G model 263A potentiostat with Powersuite software (Princeton Applied Research). A platinum counter electrode and Ag/AgCl reference electrode were used; however, all potentials quoted in this study are with respect to the SHE. A powder microelectrode (PME) was used as the working electrode which acts effectively as a cleaved mineral electrode of greater surface area (Cha, 1994). The increased surface area on a relatively small volume allows for relatively fast reaction kinetics which is important for redox processes in cyclic voltammetry that happen at a second to minute timescale. A PME is prepared by conventional glass blowing techniques and is composed of a platinum wire encased in soda lime glass with the platinum wire exposed flush to the end of the electrode. A cavity of 100 µm diameter (dictated by the diameter of the platinum wire) and ~20 µm depth is made by etching the exposed platinum in aqua regia (~80 ^{o}C) for ~2.5 hours (Renock *et al.*, 2013). The cavity is packed by tapping the electrode in PbS powdered in an agate mortar and pestle which is removed after use via sonication.

Unless otherwise stated, voltammetry was performed on freshly powdered, pristine PbS in 10 mM Na_2SeO_3 + 100 mM NaCl adjusted to pH 4.6 at 50 mV/s initiating from the open circuit potential (OCP) in the positive-going direction. The OCP (~110 mV ±5 mV) was monitored for 30 seconds before initiating each scan. Solutions of any pH were adjusted using HCl and NaOH. All reagents (excluding PbS) were obtained from Sigma Aldrich. Solutions were sparged with Ar gas for 30 minutes prior to voltammetry to remove dissolved oxygen.

On voltammograms, anodic and cathodic peaks are denoted with an ‘A’ and ‘C’, respectively. The midpoint potential (E_{mid}) of the anodic (E_A) and cathodic (E_C) peaks comprising a redox couple was defined as $E_{mid} = \frac{1}{2}(E_A + E_C)$. Peak areas and peak currents were obtained using Origin8.5 plotting software. For these purposes, peaks were defined by either the two major inflection points or local minimums or maximums bounding the peak of interest determined using a Savitzky-Golay smoothing function for 1st and 2nd derivatives. Using these bounds, peak areas were obtained through integration and peak currents by subtracting the apparent peak current from that occurring along its baseline. Unless otherwise stated, peak charges and potentials are taken from the final cycle of cyclic voltammograms.

2.3 X-ray photoelectron spectroscopy (XPS)

XPS spectra were obtained using a Kratos Axis Ultra X-ray photoelectron spectrometer with a monochromatized Al *Kα* source (1486.6 eV) primed to 8 mA and 14 kV at no more than $5 \cdot 10^{-7}$ Torr. Core spectra obtained using a 20 eV pass energy with 0.1 eV resolution were calibrated with respect to the C 1s spectrum obtained from respective samples assuming a binding energy of 284.8 eV. Peak fitting and calculation of atomic ratios were performed using CasaXPS software and the relative sensitivity factors provided. Due to the small diameter of the PME, XPS analysis was conducted on bulk PbS electrodes prepared by mounting cleaved PbS (polished to 1200 grit) to copper wire via conductive silver paste (Ted Pella Inc.) and insulated with non-conductive epoxy (Loctite). Bulk electrodes were polarized at potentials of interest (see Section 3.2) for 30 minutes in 10 mM Na_2SeO_3 + 100 mM NaCl pH 4.6. After polarization, bulk electrodes were stored in an anaerobic glove bag (5% H_2 + 95% N_2) for no more than 2 hours before being transferred into the spectrometer where evacuation could begin. Samples were not rinsed or further treated at any point after polarization. Analytical grade Na_2SeO_4, Na_2SeO_3, and Se^0 reagents (Sigma Aldrich) were used as reference standard materials.

3 RESULTS

3.1 Voltammetry

Cyclic voltammetry (CV) was performed in different scan ranges to identify the nature and kinetics of specific selenium-related redox transitions. CV performed in the scan range of [−0.65; 0.3] V exhibits 3 anodic peaks and 3 cathodic peaks (Fig. 3). Peak $\mathbf{A_1}$ is observed at ~100 mV and exhibits no change in anodic current with cycling. Rather, $\mathbf{A_1}$ assumes the same anodic current in the 1st cycle as is observed throughout the entire scan. Peak $\mathbf{C_1}$ emerges at ~ −200 mV and with cycling grows in cathodic current and shifts to ~ −100 mV where it is maintained for the remainder of the scan. Peak $\mathbf{A_2}$ emerges at −350 mV and with cycling shifts to −390 mV and decreases in anodic current. Peak $\mathbf{C_2}$ is observed at ~ −470 mV and exhibits no change in cathodic current with cycling. Peaks $\mathbf{A_3}$ and $\mathbf{C_3}$, observed at −530 and −590 mV, respectively, both grow in current magnitude, but emerge only in later cycles (typically the 10th cycle or later) suggesting some dependency upon the prior occurrence of other reactions.

CV was scanned in 1 mM Na_2SeO_3 + 100 mM NaCl pH 4.6 in the scan range of [−0.65; 0.3] V until a stable voltammogram was achieved whereupon Na_2SeO_3 was added to

increase the concentration of Se^{4+} species (Fig. 4). Current magnitudes of peaks **A_1**, **C_1**, **C_2**, **A_3**, and **C_3** increase with increasing concentration of Na_2SeO_3 which motivates attributing these peaks to selenium-related redox transitions. **A_2**, however, decreases with increasing Na_2SeO_3 concentration. This progression was also observed throughout CV in 10 mM Na_2SeO_3 + 100 mM NaCl (Fig. 3) and will be further discussed below (see Section 3.1.2).

Two anodic features are observed in the scan range of [0.0; 0.6] V (Fig. 5). **A_4** is observed at ~400 mV which increases with Na_2SeO_3 concentration attributing the feature to selenium-related activity (Fig. 6). The strong anodic currents at the upper limit comprising **A_5** are attributed to contributions from the electrode due to the bulk oxidation of PbS given by the following reaction taken from (Paul *et al.*, 1978):

$$PbS \rightarrow S^0 + Pb^{2+} + 2e^- \quad E^o = 345\ mV \qquad (R1)$$

3.1.1 Assignment of voltammetric current peaks to specific reactions

To aid reaction assignment, linear sweep voltammetry was used to isolate peaks observed with CV allowing more effective determination of peaks as either forward or reverse reactions. Successive linear sweeps scanned from 300 mV to −300 mV exhibit growth of **C_1** which, in the absence of other selenium-related reactions, indicates that **C_1** is a forward reaction (Fig. 7). Successive linear sweeps scanned from −100 mV to 300 mV exhibit no growth of **A_1**; however, **A_1** is observed in a single linear sweep from −100 mV to 300 mV if linear sweeps producing **C_1** are performed prior to the positive-going scan (Fig. 7). These results indicate that **A_1** involves the reoxidation of the species cathodically produced via **C_1** and is therefore the reverse reaction of **C_1** constituting a redox couple (denoted with **C_1**/**A_1**).

Given peak potentials of a redox couple, E_{mid} may be defined allowing a first order approximation of a formal redox potential. For the **C_1**/**A_1** couple, E_{mid} is defined as ~0.0 mV and the following half reaction taken from (Pourbaix, 1974; Saji and Lee, 2013) is proposed:

$$HSeO_3^- + 7H^+ + 6e^- \rightarrow H_2Se + 3H_2O \quad E^o = 387\ mV \qquad (R2)$$

The standard reduction potential given by Reaction R2 more appropriately describes the E_{mid} observed through voltammetry if the H^+ concentration at pH 4.6 is taken into account.

Furthermore, at the midpoint potential E_{mid}, it is assumed that the concentration of oxidants and reductants are at equilibrium. For this purpose, the Nernst equation is used given below:

$$E = E^o - \frac{59\ mV}{n} \cdot log \frac{\prod a_{reductants}}{\prod a_{oxidants}} \quad (E1)$$

where E is the potential for a given reductant to oxidant ratio, E^o is the standard reduction potential, n is the number of electrons transferred dictated by the reaction stoichiometry, and this ratio is multiplied by the log of the reaction quotient. If the standard potential is used and the Nernst equation is applied for a pH of 4.6, Reaction R2 yields a potential of 70 mV which is in good agreement with the E_{mid} of ~0.0 mV for the **C_1**/**A_1** couple. Given this assignment, **C_1** constitutes the reduction of $HSeO_3^-$ to H_2Se which is plausible given a pk_{a1} of 2.7 and a pk_{a2} 8 for the H_2SeO_3 system and 3.9 and 11 for the H_2Se system. **A_1** then constitutes the reoxidation of cathodically-produced H_2Se back to $HSeO_3^-$.

Successive linear sweeps scanned from −300 mV to −650 mV exhibit peak **C_2** in the initial sweep indicating that it is a forward reaction (Fig. 8). With additional sweeps, the magnitude of **C_2** decreases, but stabilizes at lesser cathodic currents while **C_3** emerges in later sweeps. The delayed emergence of **C_3** corroborates the observation made from (Fig. 3) that some prior reaction is necessary for **C_3** to occur which in this case indicates that **C_3** requires prior occurrence of **C_2**. These results suggest that **C_3** consumes the product of **C_2** and is therefore the subsequent reduction of the cathodic product of **C_2** to some lower oxidation state rather than the reduction of selenium initially present in solution (*i.e.*, Se^{4+} species).

A_3 is assigned to the reverse reaction of **C_3** constituting a redox couple (denoted with **C_3**/**A_3**) due to its delayed emergence concurrent with **C_3** (Fig. 3). The **C_3**/**A_3** couple possesses an E_{mid} of ~ −560 mV and the following reaction taken from (Saji and Lee, 2013) is proposed:

$$Se^0 + 2e^- + 2H^+ \rightarrow H_2Se \quad E^o = -386\ mV \quad (R3)$$

When adjusted to pH 4.6, Reaction R3 yields a potential of −639 mV which is in good agreement with the established E_{mid} of ~ −560 mV for the **C_3**/**A_3** couple. **C_3** then constitutes the reduction of Se^0 to H_2Se which is a plausible product at pH 4.6. This assignment also agrees with the

progression observed in (Fig. 8) as it requires the prior production of some Se species cathodically produced by **C₂** rather than consuming Se^{4+} species initially present in solution. **A₃** then constitutes the re-oxidation of cathodically produced H_2Se back to Se^0.

A₂ is assigned to the reverse reaction of **C₂** constituting a redox couple (denoted as **C₂**/**A₂**) due to its concurrent emergence with **C₂** (Fig. 3). The dependency of **C₃** on **C₂** and the assignment of the **C₃**/**A₃** couple to Reaction R3 suggests that **C₂** cathodically produces Se^0 available for further reduction by **C₃**. The **C₂**/**A₂** couple possesses an E_{mid} of ~ −430 mV and the reaction with the closest potential describing the reduction of Se^{4+} species to Se^0 taken from (Saji and Lee, 2013) is given below:

$$HSeO_3^- + 4e^- + 4H^+ \rightarrow Se^0 + 3H_2O \quad E^o = 779 \text{ mV} \qquad \text{(R4)}$$

If the standard potential for Reaction R4 is adjusted to pH 4.6 (using Eqn. E1), a potential of 439 mV is obtained which is an unlikely approximation for the E_{mid} of ~ −430 mV for the **C₂**/**A₂** couple. **C₂** then likely produces Se^0 by some other mechanism.

It should be noted that after a potential hold at −490 mV for 30 minutes (see Section 3.2), a red film was observed on PbS bulk electrodes characteristic of Se^0 (Chen *et al.*, 2006; Han *et al.*, 2011; Nuttal and Allen, 1984). This observation supports the suggestion that **C₂** produces Se^0 and the assignment of **C₃** to the further reduction of previously produced Se^0 to selenide via Reaction R3. A number of electrochemical studies also reporting red Se^0 have attributed its formation as a result of the conproportionation of Se^{4+} and Se^{2-} species (Espinosa, *et al.*, 1992; Kazacos and Miller, 1980; Wei *et al.*, 1994). So it is possible that the Se^0 produced via peak **C₂** occurs as a result of this process which would account for the lack of a plausible E_{mid} describing the direct reduction of Se^{4+} species to Se^0 for the **C₂**/**A₂** couple. The following reaction with the dominant Se^{4+} species at pH 4.6 is proposed:

$$HSeO_3^- + H_2Se + 2e^- + 2H^+ \rightarrow 2Se^0 + 3H_2O \qquad \text{(R5)}$$

Chemically speaking, conproportionation via Reaction R5 is plausible given that **C₂** occurs at potentials more negative than **C₁** which produces H_2Se via Reaction R2. So when potentials

comprising **C2** are induced, sufficient amounts of H_2Se have been produced to facilitate Reaction R5.

Given that **A4** is an anodic peak, its reverse reaction should occur at potentials more negative than **A4** (E < 400 mV). However, a corresponding cathodic peak is not observed with CV which complicates the assignment of **A4** due to the inability to define a plausible E_{mid}. **A4** is observed in the absence of other selenium-related activity (Fig. 5) indicating that it is a forward reaction and the oxidation of Se^{4+} species initially present in solution to Se^{6+} and the corresponding cathodic peak would be the reduction of Se^{6+} to Se^{4+}. Under this assumption, it is possible that the anodic product of **A4** is not capable of subsequent reduction due to the electrochemical inactivity of selenium in the 6+ state (Pourbaix, 1974; Saji and Lee, 2013).

To test this possibility, CV was performed in 10 mM Na_2SeO_4 + 100 mM NaCl pH 4.6 in the scan range of [−0.1; 0.6] V to observe the capacity for Se^{6+} species to be reduced (Fig. 9). This scan range was chosen to encompass potentials more negative than **A4**, but not negative enough such that potentials comprising **C1** are reached. **A4** is absent when selenium is added as Na_2SeO_4 supporting its assignment to the oxidation of Se^{4+} species to some higher oxidation state. No cathodic features are observed that could be attributed to the reduction of Se^{6+} species in agreement with electrochemical (Espinosa *et al.*, 1992; Kazacos and Miller, 1980; Lange and van den Berg, 2000) and batch chemistry studies (Han *et al.*, 2011; Han *et al.*, 2012; Jordan *et al.*, 2011) reporting the lack of reduction of Se^{6+} species. These results support the proposition that the absence of a reverse reaction of **A4** is absent due to the electrochemical inactivity of Se^{6+} although this under the assumption that **A4** is in fact the oxidation of Se^{4+} to Se^{6+}.

3.1.2 Reversibility of redox couples

By comparing the charge (in Coulombs) passed by the reverse peak (C_R) to the forward peak (C_F) of a redox couple, a charge ratio is obtained where $C_R/C_F = 1$ for an ideal, Nernstian reaction. Electron charges of a given peak are obtained by integrating the current of a peak over the applied voltage and dividing the result by the scan speed applied. As of the final cycle of (Fig. 3), the **C1**/**A1**, **C2**/**A2**, and **C3**/**A3** couples possess charge ratios of ~0.167, ~0.671, ~0.075, respectively. The $C_R/C_F < 1$ for all three couples indicates that the reverse reactions (anodic in this case) are capable of reoxidizing only a limited amount of the cathodic product of their respective forward reactions. For the **C1**/**A1** and **C3**/**A3** couples, the limited reversibility is mainly attributed to the loss of a fraction of cathodically produced H_2Se to the solution (and maybe gas)

phase which has been reported in a number of studies employing CV coupled with electrochemical quartz crystal microbalance (Cabral *et al.*, 2010; Kowalik, 2014; Solaliendres *et al.*, 2008; Wei *et al.*, 1994).

The charge ratio for the **C₂**/**A₂** couple is notably higher than that of the **C₁**/**A₁** and **C₃**/**A₃** couples which is likely given that **C₂** produces insoluble Se^0 rather than soluble H_2Se. However, it is proposed that the reversibility of the **C₂**/**A₂** couple is also affected by the solvation of H_2Se. This is due to a fraction of the cathodically produced Se^0 being further reduced to H_2Se via **C₃** which is otherwise available for reoxidation via **A₂**. This is supported by a charge ratio of ~0.855 possessed by the **C₂**/**A₂** couple in the fifth cycle of (Fig. 3) before the emergence of **C₃** compared to ~0.671 as of the final cycle after **C₃** has grown. Peak **C₂** effectively yields the same charge regardless of the presence of **C₃**. Therefore the decrease in the charge ratio is due to decreased activity of **A₂** as a result of competition with **C₃**.

3.1.3 Influence of scan rate and quantification of the reaction kinetics, pH changes, and a reaction volume using peak areas

In the case of a Nernstian reaction, the theoretical separation of peaks comprising a redox couple is $\Delta E = (59/n)$ in mV where n is the number of electrons transferred (Bard and Faulkner, 2001). If final potentials are considered (rather than potentials exhibited in initial cycles of CV scans before shift is observed), the peak separation of the **C₁**/**A₁** couple is ~200 mV which is considered rate-limited for a 6-electron transfer via Reaction R2. The peak separation of the **C₂**/**A₂** couple is ~80 mV which is also considered rate-limited if the proposed conproportionation reaction comprising **C₂** is treated as a net 2-electron transfer via Reaction R5.

Rate limitations are supported by varying the scan rate with CV in the scan range of [−0.65; 0.3] V. In the case of a Nernstian reaction, peak potentials and therefore peak separation are independent of the scan rate. The **C₁**/**A₁** and **C₂**/**A₂** couples, however, exhibit shift in potentials that increase peak separation with the root of the scan rate confirming their assignment as rate-limited (Fig. 10). Rate limitations can be caused by different processes such as a limited diffusion speed of a species to the mineral-electrode surface, or a rate-limiting adsorption reaction or electron transfer. The increase in peak separation for both redox couples is approximately linear indicating that these are not only rate-limited, but diffusion-limited

processes (Lai *et al.*, 2010) which is supported by an approximately linear dependence of the forward (in this case cathodic) peak currents with the root of the scan rate (Fig. 11) (Doi, 2014).

The peak separation for the **C₃**/**A₃** couple is ~60 mV which is considered quasi-Nernstian for a 2-electron reaction. However, an analogous assessment for the **C₃**/**A₃** couple could not be established due to their absence at scan rates greater than 50 mV/s. This is similar to the results of (Bougouma *et al.*, 2013) observing a cathodic peak attributed to the reduction of Se^0 to Se^{2-} on gold electrodes disappear at scan rates higher than 100 mV/s. It would appear that **C₃** disappears due to an insufficiently large scan range, however, the same results were observed with lower limits of −1.0 V although H_2 evolution was also observed in this case.

While the difference in potential between the cathodic and anodic peaks for a given redox couple can give some indication of which reactions are kinetically hindered and/or diffusion limited, using different reactant concentrations grants the ability to quantify reaction rates, postulate a rate equation, derive the rate constant, and even allows for rough estimates of pH changes. For these purposes, the number of moles of electrons transferred in a given peak is obtained by integrating over area of the peak comprising the forward reaction (values in A·V or C·V/s) dividing by the scan rate (to obtain values in C) and finally dividing this number by the Faraday constant (to obtain moles of electrons). Given the number of moles of electrons, the moles of all other reactants or products can be deduced by applying the stoichiometry of reactions of interest. The duration of the reaction can be approximated by the time required to scan over a given peak which is obtained by dividing the peak width (in V) by the scan rate (in V/s). The rate of the reaction is then the number of molecules produced divided by the duration of the reaction and the volume in which the reaction occurs (initially the pore volume assumed to be 1/3 of the cavity). Reaction rates for peaks assigned to specific reactions are given in (Table 1).

Also included in Table 1 are estimates of the participating PbS surface sites occupied per selenium atoms produced in the respective reactions. For this purpose, it was again assumed that one third of the cavity volume of the PME was empty while the remaining two thirds are occupied by powdered PbS. From SEM images, an average PbS cube volume was estimated to be 125 μm^3 (average grain size of about 5 µm) from which the total surface area of the powdered PbS was estimated. It was roughly assumed that one half of a grain is in contact with other grains and the other half of the estimated total surface area is actually exposed and available for

adsorption. This reactive surface area can be divided by the area occupied by one PbS surface unit using a Pb−S distance of 3 Å and, due to the cubic arrangement of atoms, resulting in a primitive surface unit cell of $3 \cdot \sqrt{2} \cdot 3 \cdot \sqrt{2} = 18$ Å^2.

To test the efficacy of reaction rate estimations, rates and corresponding rate constants were calculated for Reaction R2 at varying concentrations using Equation E2 below.

$$r = k\,[HSeO_3^-]\,[e^-]^6\,[H^+]^7 \qquad \text{(E2)}$$

Equation E2 is of the general rate law form which in this case considers reactants according to Reaction R2. For this purpose, rates, r, have been experimentally determined from CV performed in 100 mM NaCl pH 4.6 with varying concentrations of Se^{4+} (as Na_2SeO_3). From the measured rates, the resulting rate constant, k, is calculated using the experimental $[H^+]$ and the electron concentration determined from the peak position (Eh) from the CV assuming $[e^-] = 10^{-16.9 \cdot Eh}$.

Theoretically, as the selenium concentration is varied which increases the overall rate or production rate of selenide, the resulting rate constant, k, should not change; however, the calculated k values decrease (Table 2). Across multiple CV scans, there is minor shift in peak position mostly due to H^+ consumption. This minor shift in Eh and pH becomes more significant due to the exponential dependence of $[e^-]$ from Eh which results in different k values though still within the same order of magnitude. The $[H^+]$ used for the first round k calculation was simply that of the applied pH of 4.6. The smallest pH shift is expected for the lowest $HSeO_3^-$ concentration; therefore the k value obtained from the lowest $HSeO_3^-$ concentration is held constant (now k_i) to allow for estimating pH changes for any $HSeO_3^-$ concentration. This is done using the adjusted Equation E2a given below:

$$[H^+]_i = (k\,[HSeO_3^-]_i\,[e^-]_i / r_i)^{1/7} \qquad \text{(E2a)}$$

where $[HSeO_3^-]_i$ represents the various experimental $HSeO_3^-$ concentrations, $[e\text{-}]_i$ represents the electron concentration determined from the Eh of the resulting voltammogram via $[e^-] = 10^{-16.9 \cdot Eh}$, and r_i represents the corresponding reaction rate using Equation E2 while maintaining the k value obtained from the initial concentrations (see Equation E2a).

If the $[H^+]$ is recalculated for different $HSeO_3^-$ concentrations, a shift in pH is observed from 4.6 to ~4.8. This shift in pH is more than the shift expected if the consumed H^+ would

come homogeneously from the entire volume of the electrochemical cell (50 mL); in this case only about 1/10000 of the original $10^{-4.6}$ mol/l of H^+ would be consumed and now pH change would be observable. To the other extreme, the shift in pH is less than what would be expected if only the pore volume would take part in the reaction. In fact, if the latter were the case, the number of protons consumed in (Table 2) would surpass the number of protons originally available in the pore volume which would have driven up the pH to the maximum of its potential scale.

With this in mind, it is possible to quantify the actual reacting volume – that is to say, the portion of the solution that is affected by the H^+ and $HSeO_3^-$ consumption – which is expected to be greater than the pore volume used to obtain the r and the k values, but less than the total volume of the electrochemical cell. The number of moles of H^+ consumed during Reaction R2 can be determined from the number of moles of electrons yielded by CV results by maintaining the stoichiometric ratio of Reaction R2. If the number of moles of H^+ consumed during Reaction R2 is divided by the change in $[H^+]$ from the initial pH to the final pH ($10^{-4.6} – 10^{-4.82}$), a volume of $7.69 \cdot 10^{-6}$ L is obtained. If this volume is considered a hemisphere, a reactive radius of 1.2 mm is obtained with respect to the tip of the PME which is 0.1 mm in diameter (Fig. 12). This does not mean that all reactants within this radius contribute to the reaction and the ones outside do not, but rather reactants within are likely to contribute and molecules outside are not. This value may also indicate the order of magnitude of the maximum distance that a reactant has to travel in this experimental setup with selenite concentrations on the order of 0.05 mmol in order to reach the surface and obtain electrons for reduction.

3.2 XPS measurements

XPS spectra were obtained to identify the products of forward reactions observed with voltammetry described in Section 3.1. For this purpose, bulk PbS electrodes were polarized for 30 minutes in 10 mM Na_2SeO_3 + 100 mM NaCl pH 4.6 at 425 and −125 mV corresponding to peaks **A₄** and **C₁**, r espectively. Because the **C₁**/**A₁** couple is observed with the cathodic peak assuming the forward reaction (*i.e.*, the initial reaction is reduction), a potential more negative than what is observed with voltammetry was chosen to ensure sufficient potentials were applied to induce reduction. Similarly, because **A₄** is a single anodic peak, a potential more positive than what is observed with voltammetry was chosen. Given the close proximity with respect to potential and the dependency of **C₃** on **C₂**, a potential of −490 mV was also chosen. Due to

interference of the Se 3p and S 2p orbitals, selenium speciation was analyzed with respect to the Se 3d orbital (Fig. 13). In all cases peak separation is greater than the 0.1 eV resolution of the spectrometer allowing accurate attribution of different components to different oxidation states. For reference, Se 3d spectra for Na_2SeO_4, Na_2SeO_3, black Se^0, and pristine PbS standards were obtained. Due to interference from the Na 2s orbital, Na_2SeO_4 and Na_2SeO_3 standards yield peaks attributed to Na^+ at 62.6 and 62.5 eV, respectively (Rupp and Weser, 1975; Silipigni *et al.*, 2011).

3.2.1 Se 3d Spectra

PbS polarized at 425 mV yields a peak at 58.3 eV attributed to Se^{4+} in agreement with the standard spectrum value of 58.6 eV and the value of 58.2 eV as reported in (Naveau *et al.*, 2007). Similarly to what is observed in the reference spectra, an additional peak attributed to Na^+ is observed at 63.4 eV. Both Na^+ and Se^{4+} are expected as adsorbates from the 10 mM Na_2SeO_3 + 100 mM NaCl solution rather than from electrochemical production. With this in mind, the absence of any selenium component other than Se^{4+} in solution indicates the absence of any electrochemically produced selenium species.

A PbS-Se setup polarized at −125 mV yields three peaks. Peaks from non-electrochemically produced Se^{4+} and Na^+ are again present in this case at 59.1 and 63.6 eV, respectively. The peak observed at 55.6 eV is attributed to Se^0 in agreement with the standard spectrum value of 55.6 eV and the value of 55.5 eV reported in (Shenasa *et al.*, 1986); however, no visible discoloration was observed. Given that a potential of −125 mV corresponds to peak **C₁** assigned to the reduction of $HSeO_3^-$ to H_2Se via Reaction R2, the presence of the Se^0 component in this case will be further discussed in Section 4. Quantification of the selenium-related components yields relative concentrations of ~49.95% and 50.05% in favor of Se^{4+} species.

PbS polarized at −490 mV yields four peaks. The two peaks attributed to non-electrochemically produced Se^{4+} and Na^+ are observed at 58.6 and 63.0 eV, respectively. A peak at 54.7 eV is observed attributed to Se^0 which is supported by the formation of a red film as mentioned in Section 3.1.1. The fourth peak is observed as a $3d_{3/2\,-\,5/2}$ doublet at 52.6 and 53.3 eV and is attributed to Se^{2-} species in agreement with literature values of various selenides such as CdSe at 53.3 eV (Rupp and Weser, 1975) and FeSe at 53.7 eV (Hamdadou *et al.*, 2002) with respect to the higher energy component. Quantification of the selenium-related components

yields relative concentrations of ~63.4%, 12.4%, and 24.2% for Se^{4+}, Se^{0} and Se^{2-} species, respectively.

3.2.2 Pb 4f and S 2p Spectra

The Pb 4f spectra for all samples exhibit Pb $4f_{7/2–5/2}$ doublets that maintain peak intensity ratios of approximately 10:8 and peak separations of ~4.9 eV (Fig. 14). With respect to the lower energy component, the Pb $4f_{7/2}$ peaks for PbS polarized at −125 and −490 occur at binding energies ranging from 136.8 – 137.5 eV. These values are attributed to Pb^{2+} present in bulk PbS consistent with the Pb $4f_{7/2}$ peak produced by the PbS reference material. PbS polarized at 425 mV exhibits an additional peak shouldered at binding energies lower than the Pb $4f_{7/2}$ peak attributed to PbO/PbOH species formed upon oxidation of bulk PbS (Chernyshova *et al.*, 1997; Mikhlin *et al.*, 2004). The altered Pb bonding environment is supported by a shift of the Pb $4f_{7/2}$ peak to 138.0 eV.

S 2p spectra for all samples exhibit S $2p_{3/2–1/2}$ doublets at lower binding energies with an additional component at higher binding energies (Fig. 15). The doublet in all cases maintains a peak separation of ~1.3 eV and is observed, with respect to the lower energy component, from ~160.0−160.7 eV characteristic of bulk PbS S^{2-} (Buckley and Woods, 1984; Smart *et al.*, 1999). The component at higher binding energies is observed from 164.2−165.2 eV likely due to S^{0} which is typically reported in the range of 164−165 eV (De Giudici *et al.*, 2005; Scheinost *et al.*, 2008; Smart *et al.*, 1999). While assignment of oxidized sulfur components is often ambiguous, the key observation in this case is the amount of bulk sulfide which decreases from 67.35 to 56.8 to 25.4% relative to the oxidized component as the potential is increased from −490 to −125 to 425 mV, respectively.

4 DISCUSSION

In general, XPS results support the reactions assigned from voltammetric data. The absence of selenium components in any oxidation state lower than 4+ for PbS polarized at 425 mV supports the assignment of $\mathbf{A_4}$ to the oxidation of Se^{4+} to some higher oxidation state. The absence of a selenium component higher than the 4+ state suggests that the anodic product is soluble and not adsorbed to the PbS surface. Granted, Se^{4+} and Na^{+} from solution are detected indicating that soluble species can still be retained on the surface, but these occur in higher concentrations than any electrochemically produced species. The absence of a Se^{6+} component

makes it difficult to confirm Se^{6+} as a product of **A_4**, however, Se^{6+} species are soluble and would follow the above described behavior if in fact produced.

The presence of a red film after polarization at −490 in addition to a Se^0 component at 54.7 eV confirms the assignment of **C_2** as producing Se^0. The specific mechanism by which it is produced will be discussed in greater detail below. The additional presence of a Se^{2-} component suggests that during the 30 minute potential hold a fraction of the Se^0 was further reduced to Se^{2-} species in agreement with the assignment of **C_3** to Reaction R3. The presence of the mixed phase is not only in agreement with the dependency of **C_3** on **C_2**, but also plausible for a single potential given that peaks **C_2** and **C_3** are only ~120 mV apart.

From voltammetry, a fraction of the H_2Se cathodically produced via **C_3** is lost to the solution phase as indicated by the low C_F/C_R of ~0.075 yet some is available for reoxidation as indicated by the presence of peak **A_3**. It is possible that a sufficient amount of cathodically produced H_2Se does not leave the reacting volume around the PME although the Se 3d spectrum indicates that some is also retained on the electrode surface. Red Se^0 as is produced in this case has been reported capable of strongly adsorbing Se^{2-} species (Nuttall and Allen, 1984). So it is possible that retention of otherwise soluble H_2Se is due to the presence of red Se^0 in particular.

The presence of a Se^0 component after polarization at −125 mV is unexpected from voltammetry. Se^0 is known to occur in various allotropes including red monoclinic Se^0 and black (or grey) trigonal Se^0 although amorphous and colloidal forms have also been reported (Chen *et al.*, 2006; Nuttal and Allen, 1984; Scheinost *et al.*, 2008). While Se^0 components are observed after polarization at −125 and −490 mV, a red discoloration was only observed in the latter case in agreement with (Espinosa *et al.*, 1992) reporting red Se^0 formation on PbS carbon paste electrodes only if potentials were scanned below −200 mV. Furthermore, the Se^0 component observed after polarization at −490 mV is ~1.1 eV less than the component observed after polarization at −125 mV – the latter being only ~0.1 eV different than the black Se^0 reference material. These results suggest that the Se^0 observed after polarization at −125 mV is of the black variety which would not necessarily be visible on PbS.

The production of two different forms of Se^0 suggests that two different processes form them. **C_1** is assigned to produce H_2Se via Reaction R2 and the agreement between the E_{mid} of ~0.0 mV and the pH-corrected reduction potential of 70 mV is compelling. Furthermore, the low C_F/C_R of ~0.167 for the **C_1**/**A_1** couple obtained from CV suggests that the product of **C_1** is

soluble and susceptible to diffusion away from the PbS surface. This is compared to the relatively high C_F/C_R of ~0.671 for the **C_2**/**A_2** couple which has been confirmed to produce Se^0. Maintaining the assignment of Reaction R2, it is proposed that H_2Se is cathodically produced by **C_1**, but subsequently conproportionated with Se^{4+} species in solution forming black Se^0 which is then deposited on the PbS surface similarly to Se^{4+} and Na^+. This processes as well as Reaction R5 would require the production of H_2Se via **C_1** which, given that **C_2** is observed at potentials more negative than **C_1**, would occur during a potential hold both at −125 and −490 mV.

Because the conproportionation reaction producing black Se^0 occurs in solution no additional voltammetric signature would be produced either during CV or the potential hold. Furthermore, it is reasonable that this process was only allowed to occur during a 30 minute potential hold and not during the shorter timescale of CV scans where evidence of further redox transitions would be observed once deposited on the electrode surface. Via the so-called proximity effect, semiconducting minerals such as PbS have been shown capable of facilitating electronic interaction between two species that interact with surface sites even nanometers apart (Becker *et al.*, 2001; Renock and Becker, 2010; Rosso and Becker, 2003). With this in mind, the conproportionation of $HSeO_3^-$ and H_2Se molecules to form red Se^0 via Reaction R5 is mediated by the PbS surface thus yielding the cathodic peak **C_2** observed at −470 mV during CV.

The critical observation from the Pb 4f and S 2p spectra is the general lack of correlation with the Se 3d spectra. Previous XPS studies observing mackinawite (Han *et al.*, 2011; Scheinost *et al.*, 2008) and pyrite (Han *et al.*, 2012; Naveau *et al.*, 2007) surfaces after contact with Se^{4+} solutions have reported an increase in the peak areas of Fe^{3+} over Fe^{2+} and S^0 over S^{2-} components. These changes were attributed to the reduction of Se^{4+} coupled with the oxidation of the above reduced species thus resulting in enrichment of the oxidized forms. In this study, PbS S^{2-} is the most likely reductant for Se^{4+}. However, the oxidized component in the S 2p spectra attributed to S^0 decreases with the applied potential while that of PbS S^{2-} increases even though relatively electron-rich selenium species such as Se^0 and Se^{2-} are observed only at more negative potentials. Rather, the S 2p spectra is consistent with the response of S species to an applied potential in agreement with previous studies reporting the enrichment of S^0 over other S species upon anodic oxidation (Laajalehto *et al.*, 1999; Kartio *et al.*, 1998).

These results suggest that the reactions producing new selenium species do not involve the participation of Pb or S atoms. In other words, with the exception of conproportionation that

occurs in solution, the electron transfer producing red Se^0 and Se^{2-} species is merely mediated by PbS as a semiconductor. This is opposed to individual Pb or S atoms accepting or donating electrons to mediate selenium redox at the cost of redox transformation to the PbS constituents themselves.

5 CONCLUSIONS AND ENVIRONMENTAL IMPLICATIONS

Using electrochemical and spectroscopic techniques, this study has shown PbS capable of mediating a number of selenium-related redox transitions. While further work should be conducted to confirm the specific reactions induced at various potentials, the identification of any transition indicates that interactions between selenium and PbS surfaces can alter the speciation and therefore behavior of selenium in the geochemical environment.

This study has mainly focused on transitions that begin with selenium in the 4+ state, which given its solubility and therefore relative mobility is a likely species to be transported to the proximity of a PbS surface once introduced into the geochemical environment. XPS confirmation of the reduction of Se^{4+} to Se^0 and a mixed phase of Se^0 and Se^{2-} reveals that PbS is capable of not only reducing selenium, but also retaining it on the surface therefore immobilizing an otherwise mobile species. In other words, depending on the redox conditions, PbS may act as a sink for selenium if it is initially introduced as Se^{4+} species. Consideration of the reversibility of redox couples through CV reveals that a fraction of the reduced species is lost from the PbS surface through the solvation of H_2Se and is therefore not retained. Consequently, while PbS may reduce the amount of previously mobile selenium via reduction to and retention of Se^0, it may also merely facilitate a change in oxidation state (*i.e.*, Se^{2-}) without changing the mobility.

While confirmation of the anodic product of **A_4** could not be obtained, the absence of a corresponding cathodic peak comprising the anodic product's reduction in addition to the lack of any activity in 10 mM Na_2SeO_4 solution is compelling evidence for the production of an electrochemically-inactive species and therefore incapable of subsequent reduction (Espinosa *et al.*, 1992; Kazacos and Miller, 1980; Lange and van den Berg, 2000). Furthermore, the absence of any electrochemically produced selenium species in the Se 3d spectra for PbS polarized at potentials corresponding to **A_4** is in general agreement with the literature reporting weak sorption of Se^{6+} (Duc *et al.*, 2003; Martinez *et al.*, 2006). Generally speaking, results with respect to **A_4** suggest the oxidation of Se^{4+} to Se^{6+}. Under this assumption, PbS is then capable of facilitating a

redox transition to a species that appears incapable of subsequent transition and would therefore remain in a soluble and mobile state. Given these results, it is understandable why Se^{6+} species often dominate natural waters.

While the identification of redox transitions elucidates the capacity of PbS to mediate such reactions, further work should be conducted to gain a greater understanding of the participation of the PbS substrate. For example, the midpoint potentials observed in this study deviate from standard reduction potentials even when corrected for the appropriate experimental conditions. This may be an indicator of incorrect assignment, however, it is also possible that properties inherent to the PbS substrate allow for reactions to occur at potentials more negative of positive than what is theoretically predicted (*i.e.*, under or overpotentials). Understanding the tendency for PbS to cause such deviations from theoretical potentials is then critical in predicting whether or not a selenium redox transition will occur under various environmental conditions and may warrant the need to consider potentials unique to PbS interactions.

Furthermore, XPS spectra of Pb and S reveal no changes to the Pb and S environment suggesting that PbS has acted as a semiconducting substrate facilitating the transfer of electrons rather than the transfer of electrons involving a change oxidation state of the substrate itself. These results then indicate that any selenium-related redox transitions would not induce the dissolution of PbS, which would otherwise introduce Pb ions into the environment. These results, however, may be due to the fact that redox transitions have been induced by an applied potential. So it would be valuable to corroborate the results of this study with batch chemistry or sorption techniques where specific potentials are not induced upon the system. Such comparison would help in understanding the source and sink of electrons transferred in observed reactions.

This study has also provided a novel assessment of reaction kinetics strictly using voltammetric data. From this data, the estimation of a reaction volume, radius, and changes in pH within elucidate the need for considering reactions that occur at mineral surfaces with respect to proximity to the surface. This assessment may provide insight into, for example, geochemical processes that occur in sediment pores or subsurface environments. Given this reaction volume, the limited reversibility of the redox transitions due to solvation of H_2Se reveals that cathodically produced H_2Se is capable of diffusing a significant distance from the mineral surface.

Finally, this study has exemplified the combination of electrochemical and spectroscopic techniques that is not commonly utilized in geochemical studies. While the use of batch

chemistry or sorption techniques prior to spectroscopic analysis is a powerful technique to observe mineral-mediated redox transitions, the use of electrochemical preparation instead allows the ability to quantify various aspects of transitions such as potential, reversibility, and even the moles produced in addition to allowing an attempt to assign specific reactions.

ACKNOWLEDGEMENTS

First and foremost I would like to thank Dr. Udo Becker for allowing me to pursue this challenging and rewarding opportunity. He has always given me encouragement and support above all helping me learn how to learn for which I will always be grateful. I also thank Dr. Ke Yuan and Youngjae Kim for their vital discussions on the foreign subject of electrochemistry and sharing in the headaches that followed shortly thereafter. Xièxiè shifus. Finally, I thank the Department of Energy, Heavy Element Chemistry, grant DE-FG02-06ER15783 for support allowing the ability to conduct the necessary tasks in order to accomplish this work.

REFERENCES

Bard A. J. and Faulkner L. R. (2001) Electrochemical methods fundamentals and applications. *John Wiley and Sons, Inc.*

Becker U., Rosso K. M. and Hochella, Jr. M. F. (2001) The proximity effect on semiconducting mineral surfaces: a new aspect of mineral surface reactivity and surface complexation theory? *Geochim. Cosmochim. Acta* **65**, 2641–2649.

Bougouma M., Van Elewyck A., Steichen M., Buess-Herman C. and Doneux T. (2013) Selenium electrochemistry in choline chloride – urea deep eutectic electrolyte. *J. Solid State Electrochemistry* **17**, 527–536.

Buckley A. N. and Woods R. (1984) An x-ray photoelectron spectroscopic study of the oxidation of galena. *Appl. Surf. Sci.* **17**, 401–414.

Cabral M. F., Pedrosa V. A. and Machado S. A. S. (2010) Deposition of selenium thin layers on gold surfaces from sulphuric acid media : Studies using electrochemical quartz crystal microbalance, cyclic voltammetry and AFM. *Electrochim. Acta* **55**, 1184–1192.

Cha C. S., Li C. M., Yang H. X. and Liu P. F. (1994) Powder microelectrodes. *J. Electroanal. Chem.* **368**, 47–54.

Chen Y., Li L., Ulivo A. D. and Belzile N. (2006) Extraction and determination of elemental selenium in sediments — A comparative study. *Analytica Chim. Acta* **577**, 126–133.

Chernyshova I. V and Andreev S. I. (1997) Spectroscopic study of galena surface oxidation in aqueous solutions I. Identification of surface species by XPS and ATR / FTIR spectroscopy. *Appl. Surf Sci*. **108**, 225-236

Clark S. K. and Johnson T. M. (2010) Selenium stable isotope investigation into selenium biogeochemical cycling. *J. Environ. Qual.* **39**, 2200–2210.

Curti E., Aimoz L. and Kitamura A. (2013) Selenium uptake onto natural pyrite. *J. Radioanal. Nucl. Chem.* **295**, 1655–1665.

De Giudici G., Rossi A., Fanfani L. and Lattanzi P. (2005) Mechanisms of galena dissolution in oxygen-saturated solutions: Evaluation of pH effect on apparent activation energies and mineral-water interface. *Geochim. Cosmochim. Acta* **69**, 2321–2331.

Dhillon S. K. and Dhillon K. S. (2000) Selenium adsorption in soils as influenced by different anions. *J. Plant Nutr. Soil Sci.* **163**, 577–582.

Doi R. (2014) Determination of the selenium (VI)/(IV) standard redox potential by cyclic voltammetry. *J. Nucl. Sci. Technol.* **51**, 56–63.

Dubrovsky N. M., Neil J. M., Fujii R., Oremland R. S. and Hollibaugh J. I. (1990) Influence of redox potential on selenium distribution in groundwater, Mendota, western San Joaquin Valley, California. *U.S Geol. Surv.* **6439-79**, 90–138.

Duc M., Lefevre G., Fedoroff M., Jeanjean J., Rouchaud J. C., Monteil-Rivera F., Dumonceau J. and Slobodan M. (2003) Sorption of selenium anionic species on apatites and iron oxides from aqueous solutions. *J. Environ. Radioact.* **70**, 61–72.

Espinosa A. M., Tascón M. L., Vásquez M. D. and Batanero P. S. (1992) Electroanaytical study of selenium (+IV) at a carbon paste electrode with electrolytic binder and electroactive compound incorporated. *Electrochim. Acta* **37**, 1165–1172.

Feliu J. M., Gómez R., Llorca M. J. and Aldaz A. (1993) Electrochemical behavior of irreversibly adsorbed selenium dosed from solution on Pt (h, k, l) single crystal electrodes in sulphuric and perchloric acid media. *Surf. Sci.* **289**, 152–162.

Martínez M., Giménez J., de Pablo J., Rovira L. and Duro L. (2006) Sorption of selenium (IV) and selenium (VI) onto magnetite. *Appl. Surf. Sci*. **252**, 3767–3773.

Hamdadou N., Bernede J. C. and Khelil A. (2002) Preparation of iron selenide films by selenization technique. *J. Cryst. Growth* **241**, 313–319.

Han D. S., Batchelor B. and Abdel-wahab A. (2012) Sorption of selenium (IV) and selenium (VI) onto synthetic pyrite (FeS2): spectroscopic and microscopic analyses. *J. Colloid Interface Sci.* **368**, 496–504.

Han D. S., Batchelor B. and Abdel-wahab A. (2013) XPS Analysis of Sorption of Selenium (IV) and Selenium (VI) to Mackinawite (FeS). *Environmental Progress and Sustainable Energy* **32**, 84–93.

Ivandini T. A. and Einaga Y. (2013) Electrochemical detection of selenium (IV) and (VI) at gold-modified diamond electrodes. *Electrocatalysis* **4**, 367–374.

Jordan N., Foerstendorf H., Weiß S., Heim K., Schild D. and Brendler V. (2011) Sorption of selenium (VI) onto anatase : macroscopic and microscopic characterization. *Geochim. Cosmochim. Acta* **75**, 1519–1530.

Kartio I. J., Laajalehto K., Suonin E. J., Buckley A. N., Woods R. (1998) The initial products of the anodic oxidation of galena in acidic solution and the influence of mineral stoichiometry. *Colloids and Surfaces* **133**, 303–311.

Kazacos M. S. and Miller B. (1980) Studies in selenious acid reduction and CdSe film deposition. *J. Electrochemical Soc. Electrochem. Sci. Technol.* **127**, 869–873.

Kim B. S., Hayes R. A., Prestidge C. A. and Smart R. S. C. (1994) Scanning tunnelling microscopy studies of galena: the mechanism of oxidation in air. *Appl. Surf. Sci.* **78**, 385–397.

Kowalik R. (2014) Microgravimetric studies of selenium electrodeposition onto different substrates. *Arch. Metall. Mater.* **59**, 45–47.

Laajalehto K., Kartio I., Heinonen M. and Laiho T. (1999) Temperature controlled photoelectron spectroscopic investigation of volatile species on PbS (100) Surface. *Proc. Int. Conf. SRMS-2 Japan J. Appl. Phys.* **38**, 265–268.

Lai Y., Liu F., Li J., Zhang Z. and Liu Y. (2010) Nucleation and growth of selenium electrodeposition onto tin oxide electrode. *J. Electroanal. Chem.* **639**, 187–192.

Lange B. and Berg C. M. G. Van Den (2000) Determination of selenium by catalytic cathodic stripping voltammetry. *Analytica Chim. Acta* **418**, 33–42.

Maranowski B., Strawski M., Osowiecki W. and Szklarczyk M. (2015) Study of selenium electrodeposition at gold electrode by voltammetric and rotating disc electrode techniques. *J. Electroanal. Chem.* **752**, 54–59.

Martínez-Torrents A., Giménez J., Martínez-Lladó X., de Pablo J. and Casas I. (2015) Incorporation of selenium (IV) and selenium (VI) on uranyl peroxide. *J. Radioanal. Nucl. Chem.* **303**, 153–159.

Mikhlin Y., Kuklinskiy A., Mikhlina E., Kargin V. and Asanov I. (2004) Electrochemical behaviour of galena (PbS) in aqueous nitric acid and perchloric acid solutions. *J. Appl. Electrochemistry* **34**, 37–46.

Naftz D. and Rice J. (1989) Geochemical processes controlling selenium in ground water after mining, Powder River Basin, Wyoming, U.S.A. *Appl. Geochemistry* **4**, 565–575.

Naveau A., Monteil-rivera F., Guillon E. and Dumonceau J. (2007) Interactions of aqueous selenium (-II) and (IV) with metallic sulfide surfaces. *Environ. Sci. Technol.* **41**, 5376–5382.

Nuttall K. L. and Allen F. S. (1984) Hydrogen selenide ion adsorption to colloidal elemental selenium. *Inorganica Chim. Acta* **89**, 199–201.

Paul R. L., Nicol M. J., Diggle J.. W. and Saunders A. P. (1977) The electrochemical behaviour of galena (lead sulphide) - I. anodic dissolution. *Electrochim. Acta* **23**, 625–633.

Pourbaix M. (1974) Atlas of electrochemical equilibria in aqueous solutions. *National Association of Corrosion Engineers*

Renock D. and Becker U. (2010) A first principles study of the oxidation energetics and kinetics of realgar. *Geochim. Cosmochim. Acta* **74**, 4266–4284.

Renock D., Mueller M., Yuan K., Ewing R. C. and Becker U. (2013) The energetics and kinetics of uranyl reduction on pyrite, hematite, and magnetite surfaces: a powder microelectrode study. *Geochim. Cosmochim. Acta* **118**, 56–71.

Rosso K. M. and Becker U. (2003) Proximity effects on semiconducting mineral surfaces II : distance dependence of indirect interactions. *Geochim. Cosmochim. Acta* **67**, 941–953.

Rupp H. and Weser U. (1975) X-Ray photoelectron spectroscopy of some selenium containing amino acids. *Bioinorg. Chem.* **5**, 21–32.

Saji V. and Lee C. (2013) Selenium electrochemistry. *RSC Adv.* **3**, 10058–10077.

Santos M. C. and Machado S. A. S. (2004) Microgravimetric, rotating ring-disc and voltammetric studies of the underpotential deposition of selenium on polycrystalline platinum electrodes. *J. Electroanal. Chem.* **567**, 203–210.

Scheinost A. C., Kirsch R., Banerjee D., Fernandez-martinez A., Zaenker H., Funke H. and Charlet L. (2008) X-ray absorption and photoelectron spectroscopy investigation of selenite reduction by Fe II -bearing minerals. *J. Contam. Hydrol.* **102**, 228–245.

Shenasa M., Sainkar S. and Lichtman D. (1986) XPS study of some selected selenium compounds. *J. Electron Spectrosc.* **40**, 329–337.

Silipigni L., Schirò L., Scolaro L. M., Luca G. De and Salvato G. (2011) The XPS and XAES spectra of Na1. *Appl. Surf. Sci.* **257**, 10888–10892.

Smart R. S. C., Skinner W. M. and Gerson A. R. (1999) XPS of sulphide mineral surfaces: metal-deficient, polysulphides, defects and elemental sulphur. **105**, 101–105.

Solaliendres M., O., Manzoli A., Salazar-Banda G. R., Eguiluz K. I. B., Tanimoto T. and Machado S. A. S. (2008) The processes involved in the Se electrodeposition and dissolution on Au electrode: the H_2Se formation. *J. Solid State Electrochemistry* **12**, 679–686.

Wei C., Myung N. and Rajeshwar K. (1994) A combined voltammetry and electrochemical quartz crystal micriogravimetry study of the of aqueous Se(IV) at gold. *J. Electroanal. Chem.* **375**, 109–115.

Wittstock G., Kartio I., Hirsch D., Kunze S. and Szargan R. (1996) Oxidation of galena in acetate buffer investigated by atomic force microscopy and photoelectron spectroscopy. *Langmuir* **12**, 5709–5721.

Wu L. (2004) Review of 15 years of research on ecotoxicology and remediation of land contaminated by agricultural drainage sediment rich in selenium. *Ecotoxicol. Envrionmental Saf.* **57**, 257–269.

Yudovich Y. E. and Ketris M. P. (2006) Selenium in coal : a review. *Int. J. Coal Geol.* **67**, 112–126.

Tables

Table 1. Estimated reaction rates obtained from the final cycle of the cyclic voltammogram observed in (Fig. 3). Rates were estimated with respect to the moles of selenium produced by the given reaction. Additionally included is the sites occupied per produced selenium atom.

Peak	Reaction	Rate, r ($\frac{\text{moles}}{\text{L}\cdot\text{s}}$)	Sites/Atom
C_1	2	0.0101	0.0996
C_2	3	0.0068	0.5308
C_3	5	0.0102	0.6804

Table 2. Estimated reaction rates and resulting rate constant obtained with varying concentrations of Se^{4+} calculated with respect to the moles of selenium produced via Reaction R2.

$[HSeO_3^-]$ (mM)	Rate (r) (mmol/(Ls))	Eh (mV)	k (fixed pH=4.6) $s^{-1}mol^{-13}$	pH (fixed k= $8.9\cdot10^{20}$ $s^{-1}mol^{-13}$)
10	10.1	111	$8.9\cdot10^{20}$	4.60
15	11.2	111	$6.6\cdot10^{20}$	4.62
20	12.2	111	$5.3\cdot10^{20}$	4.63
25	12.5	114	$2.2\cdot10^{20}$	4.69
30	13.2	113	$2.4\cdot10^{20}$	4.68
35	13.9	119	$5.4\cdot10^{19}$	4.77
40	14.0	121	$3.0\cdot10^{19}$	4.81
45	14.8	121	$2.8\cdot10^{19}$	4.81
50	15.5	121	$2.6\cdot10^{19}$	4.82
55	16.2	117	$6.4\cdot10^{19}$	4.76

Figures

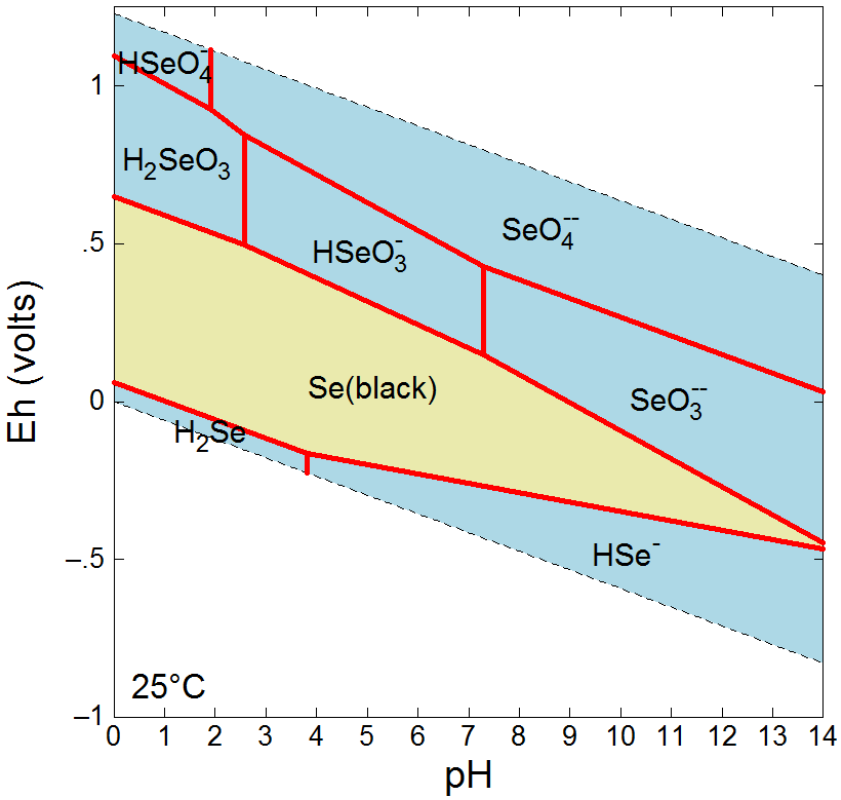

Fig 1: Eh-pH diagram for selenium at 10 mM, 25 ºC

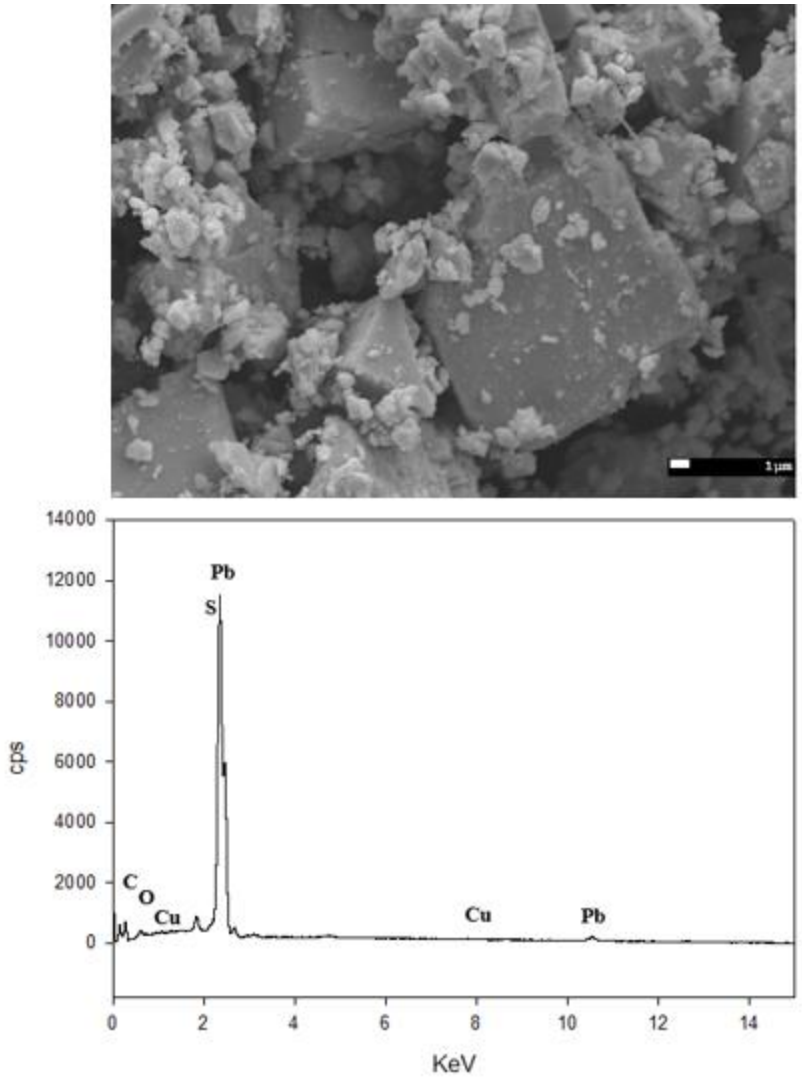

Figure 2: SEM/EDS image of powdered PbS (*above*) and the resulting spectra (*below*). In addition to Pb and S, Cu was detected which is an impurity commonly reported for PbS sourced from Missouri.

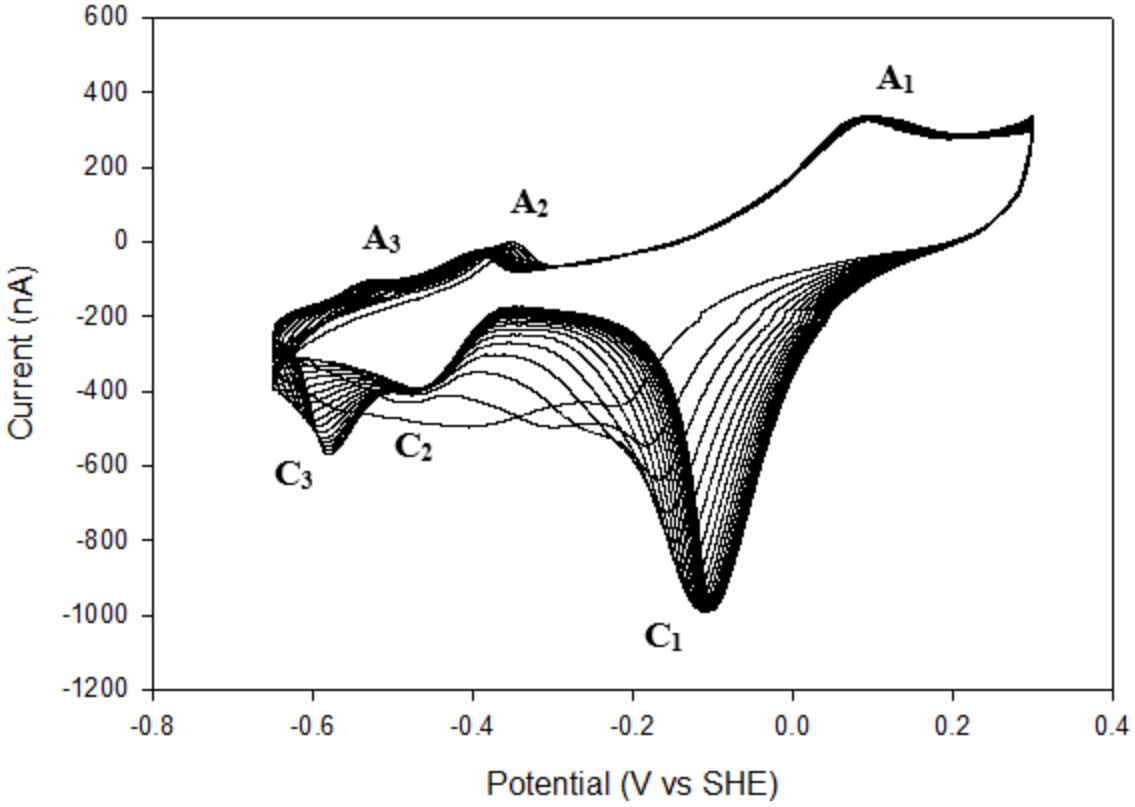

Fig. 3: Cyclic voltammogram of PbS in 100 mM NaCl + 10 mM Na_2SeO_3 pH 4.6. The scan was initiated from the OCP at 50 mV/s in the positive-going direction. Shown are 20 cycles. Peaks labeled with 'A' represent anodic features while peaks labeled 'C' represent cathodic peaks.

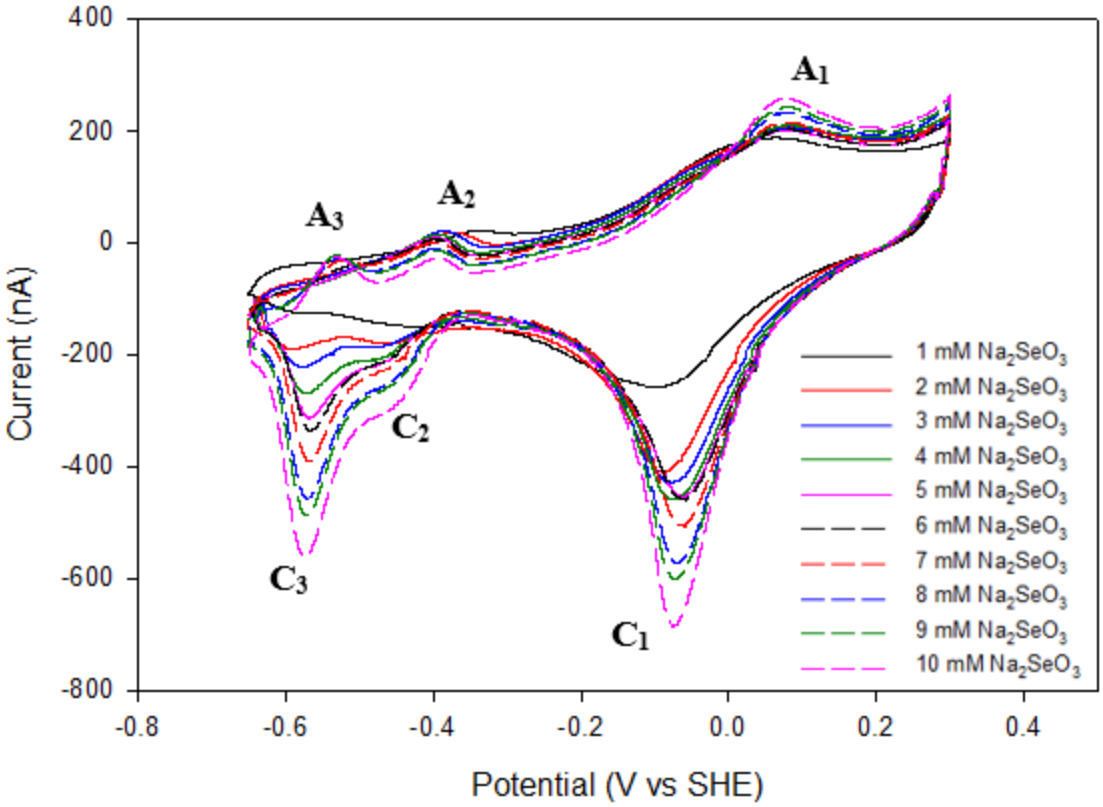

Fig. 4: Overlayed cyclic voltammograms of PbS in 100 mM NaCl pH 4.6 with varying concentrations of Na_2SeO_3 (see inset). Scans were initiated from the OCP in the positive direction at 50 mV/s. Shown are the final cycles of each scan. **A_1**, **C_1**, **C_2**, **A_3**, and **C_3** increase in current magnitude indicating that they are selenium-related redox processes. **A_2** decreases in current magnitude which is discussed in section 3.1.2.

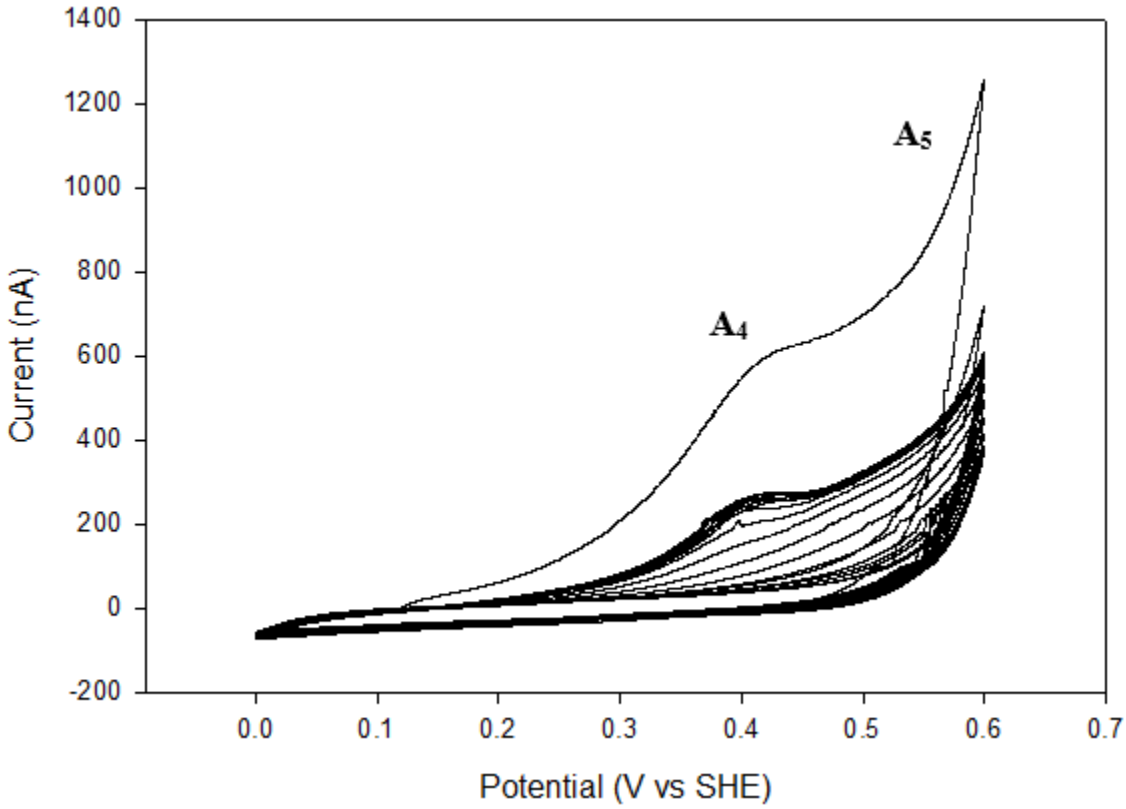

Fig. 5: Cyclic voltammogram of PbS in 100 mM NaCl + 10 mM Na_2SeO_3 pH 4.6. The scan was initiated from the OCP in the positive direction at 50 mV/s. **A_4** is observed at its greatest anodic current in the initial cycle and its least in the 2nd cycle. With continued cycling **A_4** grows and stabilizes at an anodic current less than the initial cycle. Anodic contributions from the bulk oxidation of the PbS electrode (**A_5**) are observed at the upper scan limit.

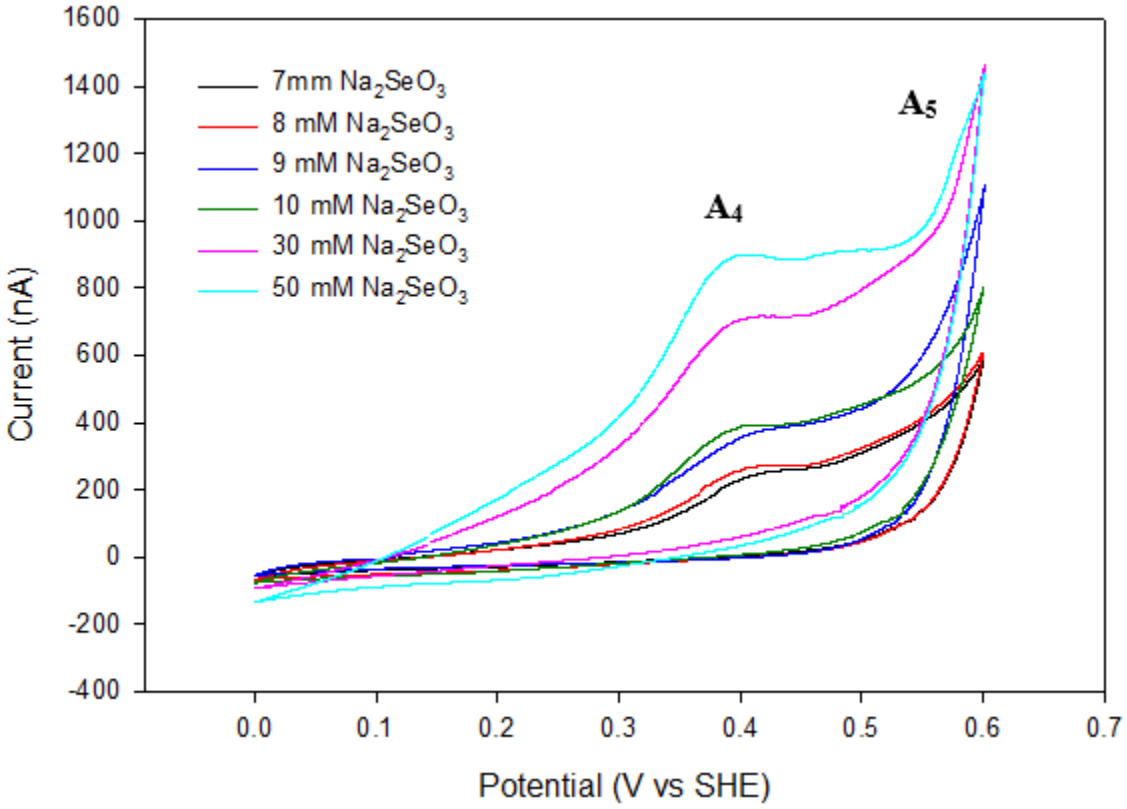

Fig. 6: Separate cyclic voltammograms of PbS in 100 mM NaCl pH 4.6 with varying concentrations of Na_2SeO_3 (see inset). Scans were initiated from the OCP in the positive direction at 50 mV/s. **A_4** increases anodic currents with increasing Na_2SeO_3 concentration indicating it is a selenium-related reaction

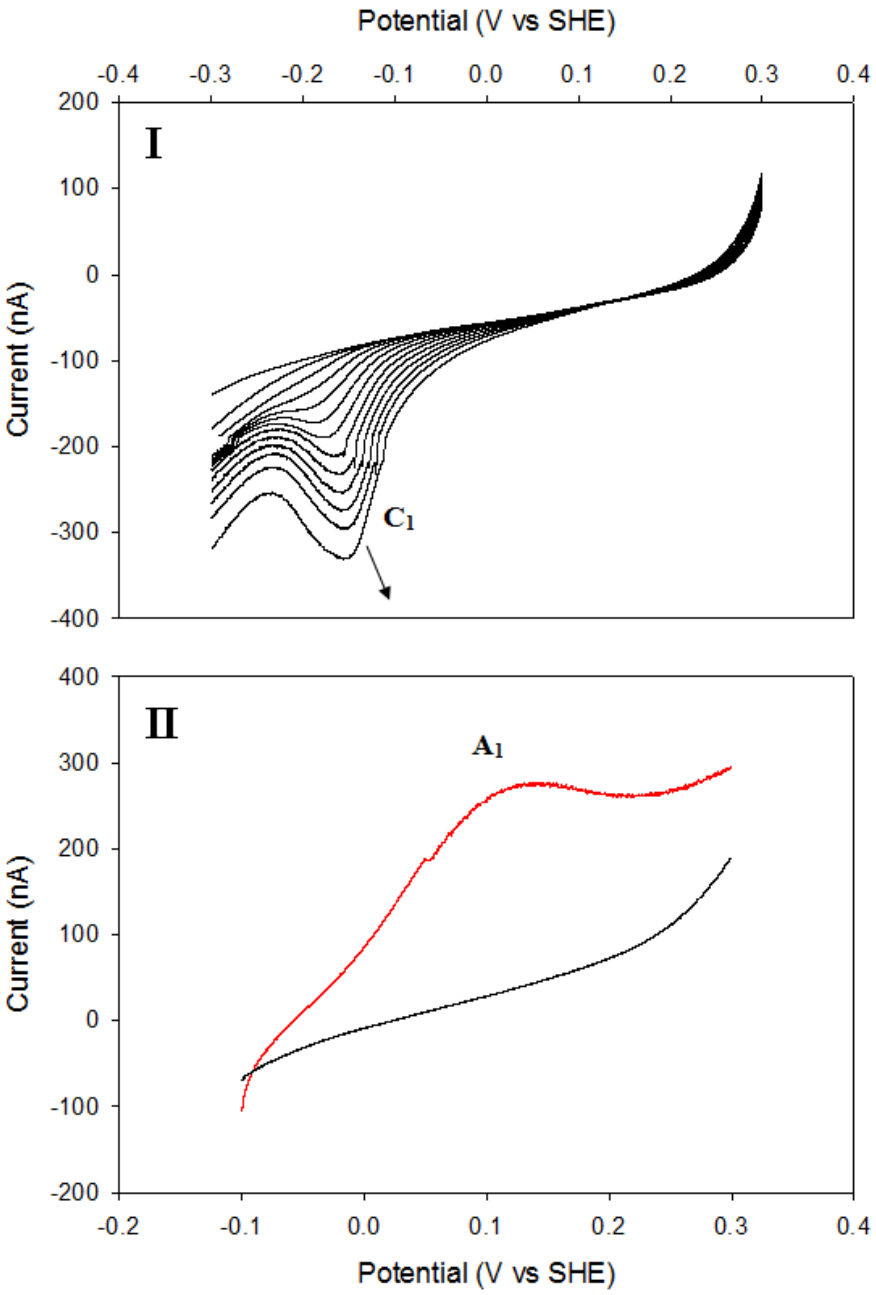

Fig. 7: (**I**) Successive negative-going linear sweeps of PbS in 100 mM NaCl + 10 mM Na_2SeO_3 pH 4.6 at 50 mV/s. As indicated by the arrow, $\mathbf{C_1}$ grows with successive sweeps which in the absence of other selenium-related peaks indicates that it consumes selenium as is initially present in solution (i.e. Se^{4+}). (**II**) Positive-going linear sweeps of separate PbS powders in 100 mM NaCl + 10 mM Na_2SeO_3 pH 4.6 at 50 mV/s performed without prior voltammetry (black) and after the scans shown in (**I**) were performed (red) whereupon $\mathbf{A_1}$ emerges. The emergence of $\mathbf{A_1}$ only after $\mathbf{C_1}$ is produced indicates that it is the reverse reaction of $\mathbf{C_1}$. Note the different axes scales.

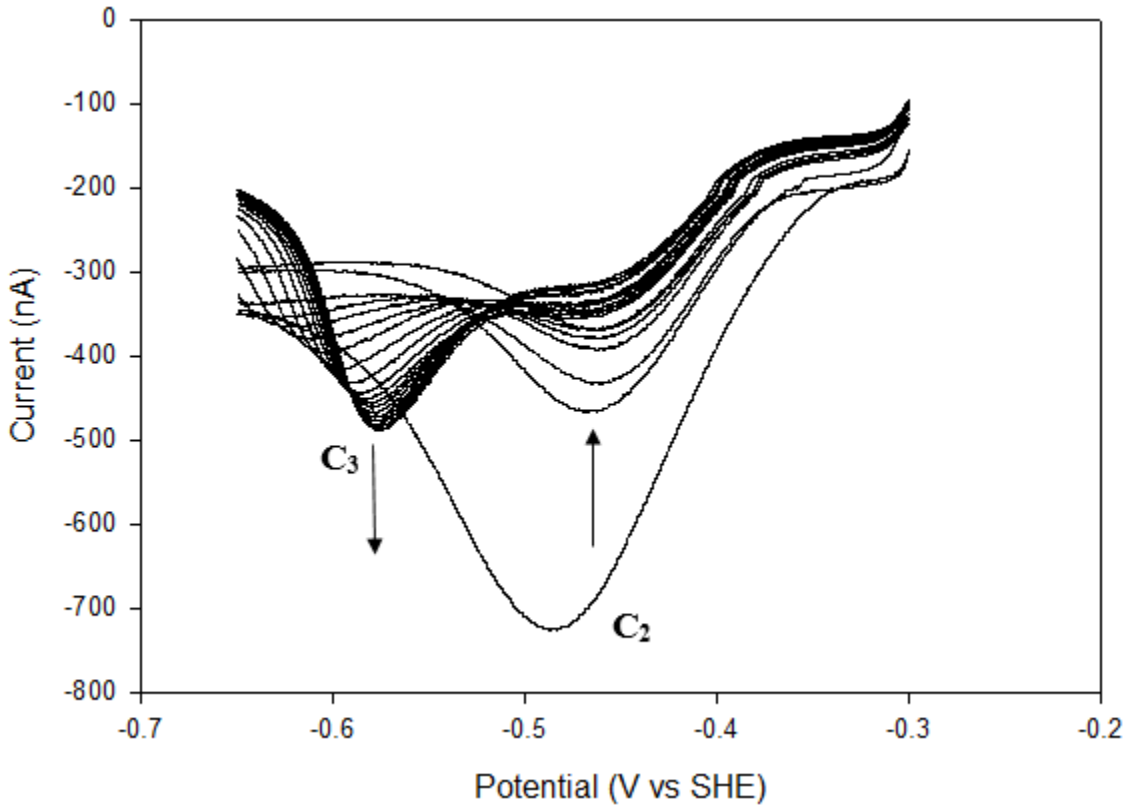

Fig. 8: Successive linear sweeps of PbS in 100 mM NaCl + 10 mM Na_2SeO_3 pH 4.6. Sweeps were scanned from -500 mV to -850 mV at 50 mV/s. **C_2** is observed in the initial sweep indicating that it consumes reactant initially present in solution (i.e. Se^{4+}). **C_3** is observed to emerge only in later sweeps indicating that it is dependent upon prior occurrence of **C_2**. The growth of **C_3** with the concurrent decay of **C_2** as indicated by the arrows suggests that **C_3** consumes the product of **C_2**.

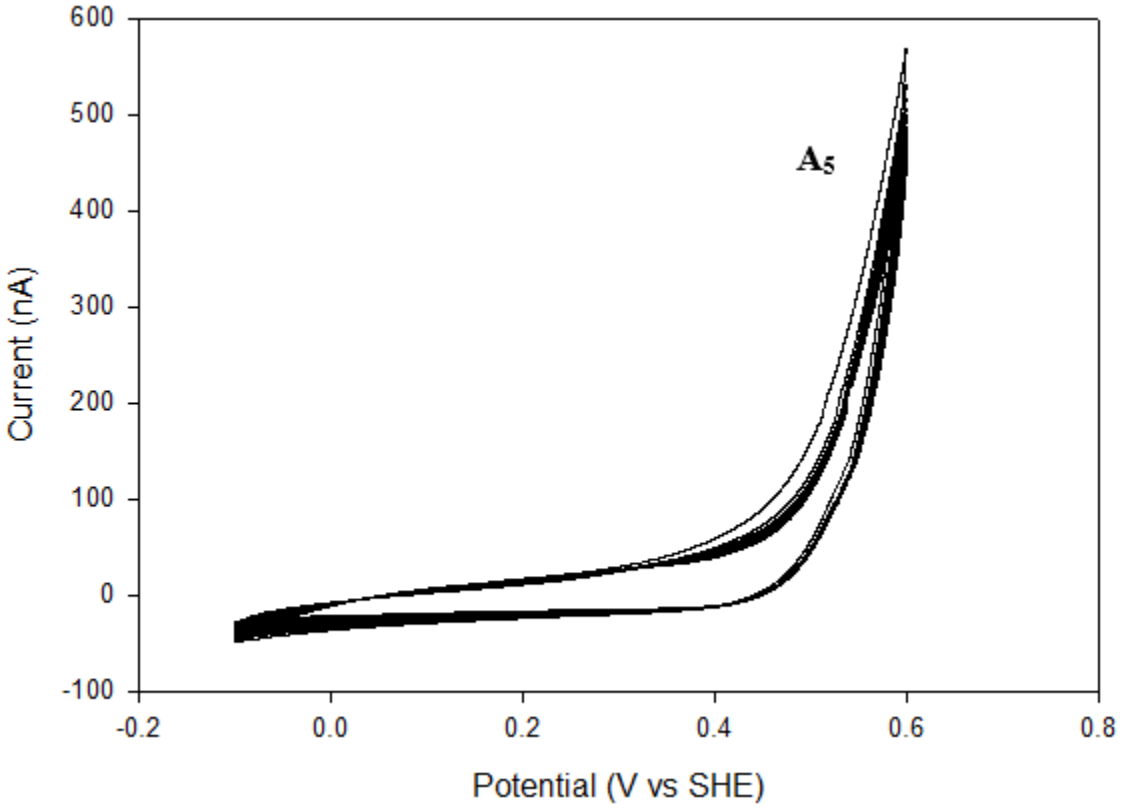

Fig. 9: Cyclic voltammograms of PbS in 100 mM NaCl + 10 mM Na_2SeO_4 (Se^{6+}) pH 4.6. The scan was initiated from the OCP in the positive direction at 50 mV/s. Shown are 20 cycles. No cathodic feature attributable to the reduction of Se^{6+} is observed in any cycle.

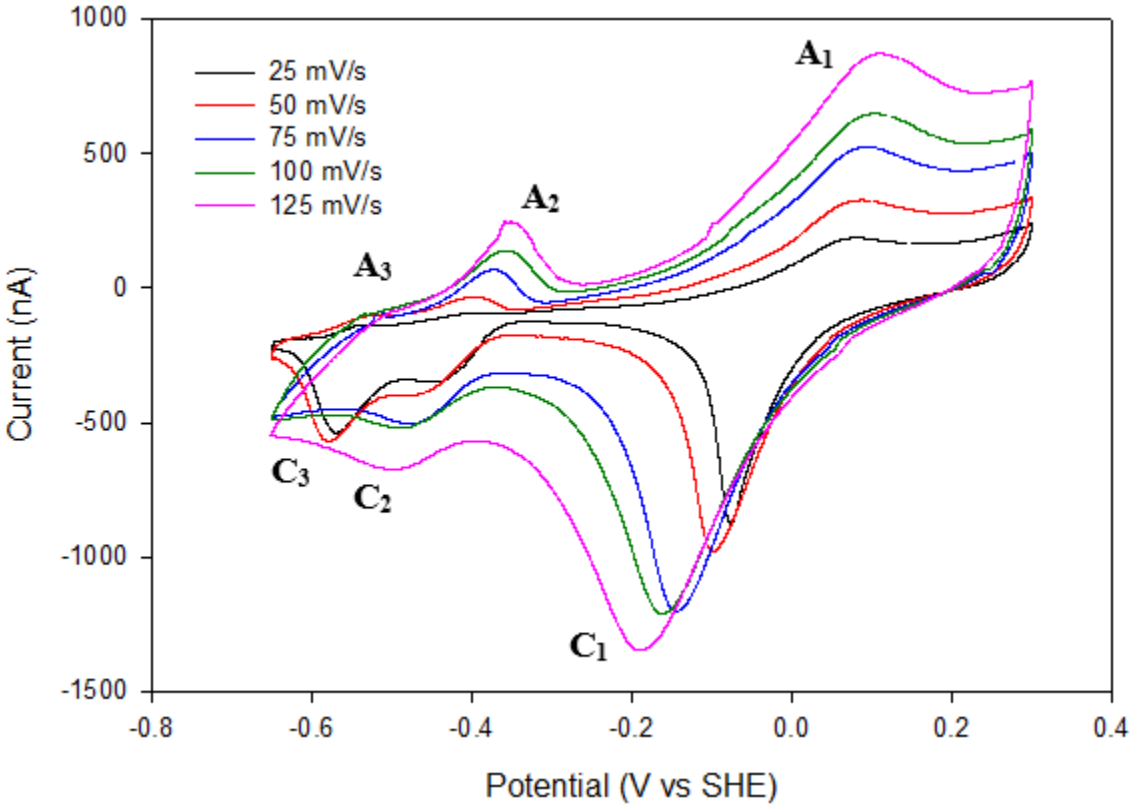

Fig. 10: Separate cyclic voltammograms of PbS in 100 mM NaCl + 10 mM Na_2SeO_3 pH 4.6 with varying scan rates (see inset). Scans were initiated from the OCP in the positive direction. Shown are the final cycles of each scan. **A_1**, **C_1**, **A_2**, and **C_2** grow with faster scan rates while **A_3** and **C_3** are absent with scan rates faster than 50 mV/s.

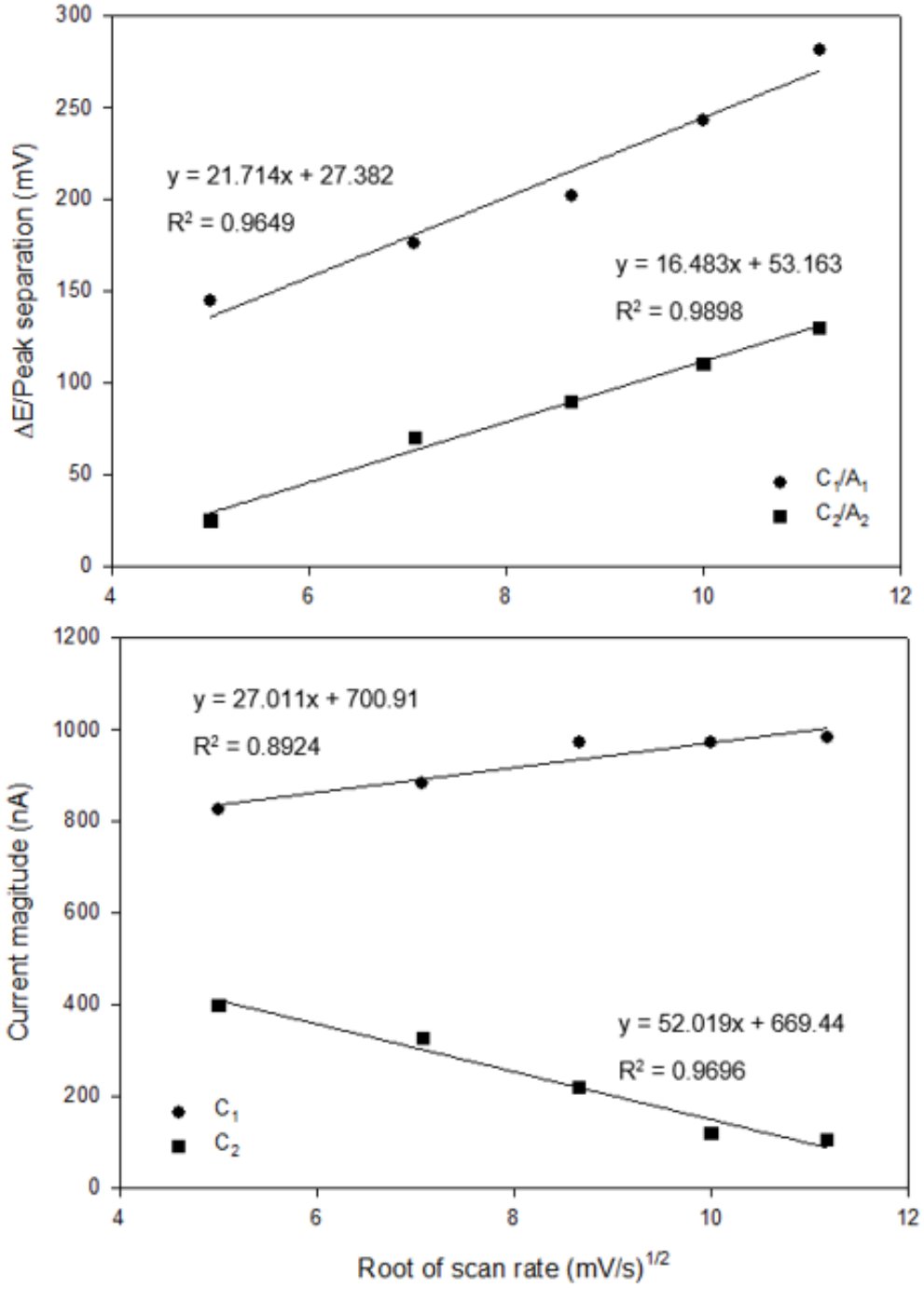

Fig. 11: (top) ΔE as a function of the root of the scan rate for the **C_1/A_1** and **C_2/A_2** redox couples and (bottom) current magnitude of **C_1** and **C_2** as a function of scan rate with least-squares fit provided for each plot. Peak potentials and current magnitudes were taken from Fig. 10.

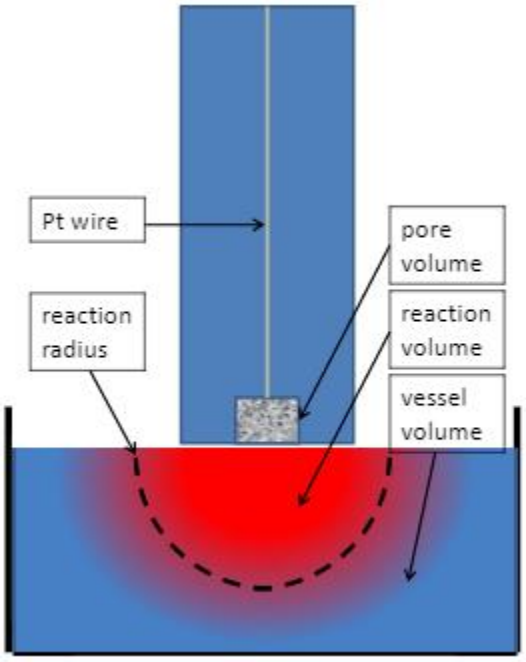

Fig. 12: Schematic of the PME submerged in an electrochemical cell. The dotted line represents the estimated reacting volume with respect to the tip of the PME which is subject to a gradient of $[H^+]$ and $[HSeO3^-]$ consumed during Reaction R2 represented by the various intensities of red.

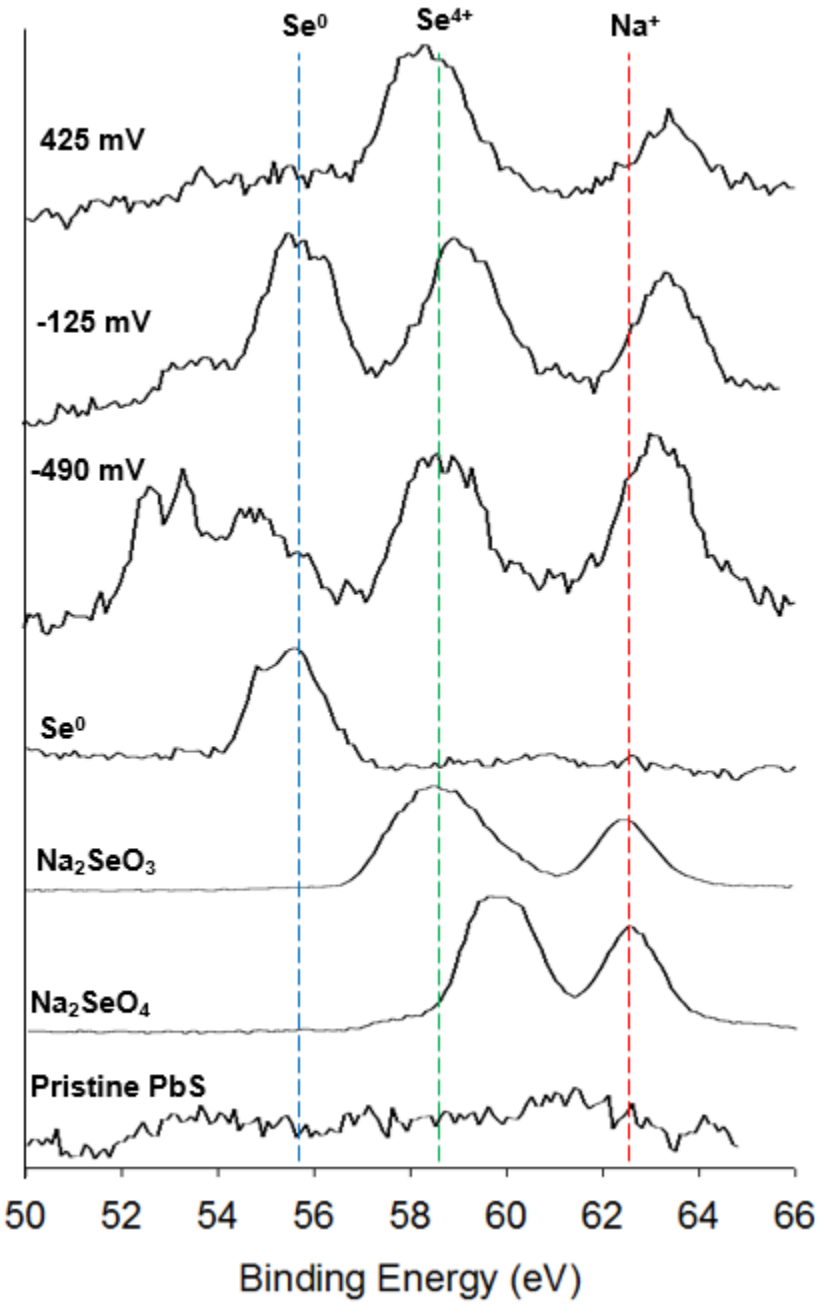

Fig. 13: Se 3d spectra of PbS samples polarized at 425, −125, and −490 mV in 10 mM Na_2SeO_3 + 100 mM NaCl pH 4.6 for 30 minutes. The dotted lines show the binding energies of components from Se^0, Na_2SeO_3, and Na_2SeO_4 reference materials that also appear in sample spectra.

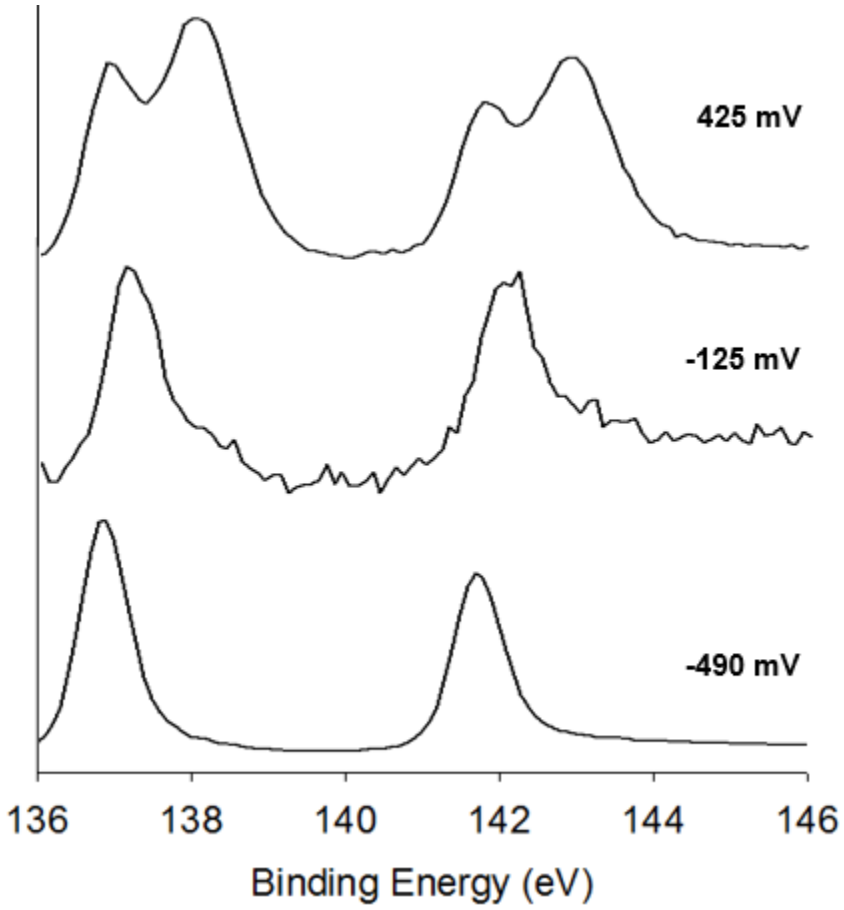

Fig. 14: Pb 4f spectra of PbS samples polarized 425, −125, and −490 mV in 10 mM Na_2SeO_3 + 100 mM NaCl pH 4.6 for 30 minutes.

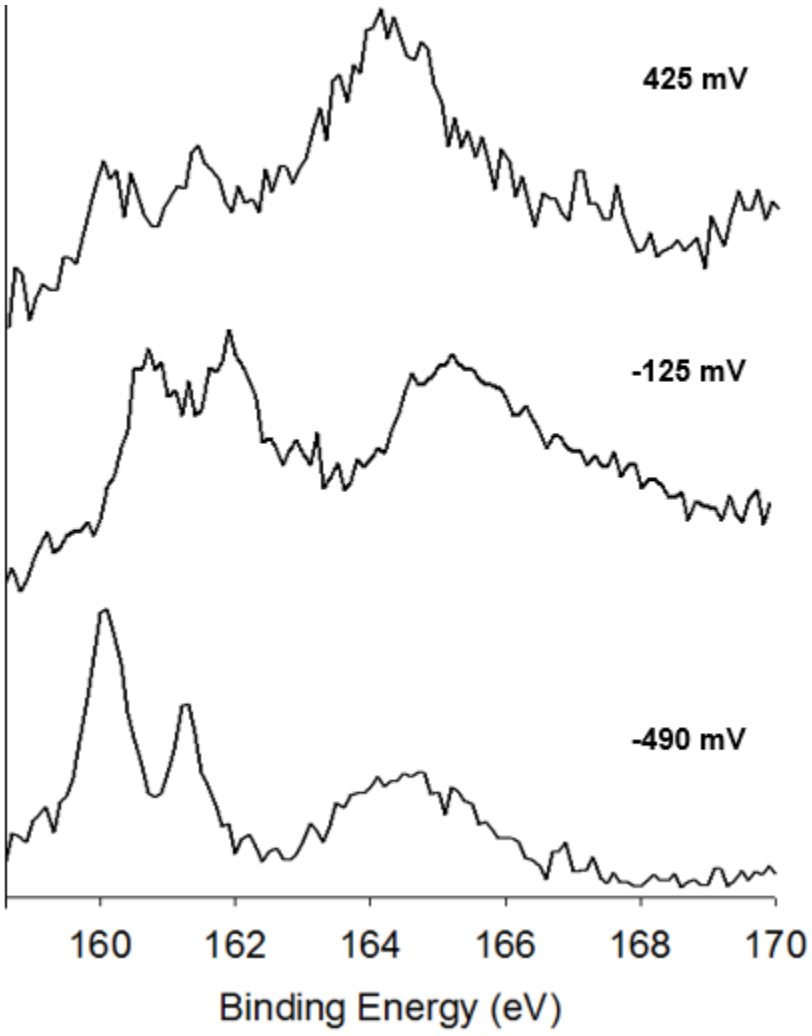

Fig. 15: S 2p spectra of PbS samples polarized 425, −125, and −490 mV in 10 mM Na_2SeO_3 + 100 mM NaCl pH 4.6 for 30 minutes.